MOIRÉ FRINGES IN UNDERWATER ACOUSTICS

by

MICHAEL RICHARD NOBLE

A THESIS SUBMITTED IN PARTIAL FULFILLMENT

OF THE REQUIREMENTS FOR THE DEGREE OF

MASTER OF SCIENCE

in the Department

of

Physics

ACCEPTED
FACULTY OF GRADUATE STUDIES

DEAN

DATE May 7th 1974

We accept this thesis as conforming

to the required standard

© MICHAEL RICHARD NOBLE, 1974

UNIVERSITY OF VICTORIA

APRIL 1974

All rights reserved. This thesis may not be reproduced in whole or in part, by mimeograph or other means, without the permission of the author.

Supervisor: Dr. W.M. Barss

ABSTRACT

Reverberation (non-specular reflection) of sound from a floating ice sheet was studied by means of models. The ice layer was represented by plane and corrugated sheets of glass and plastic. Data were obtained in the form of charts showing reverberant energy as a function of both angle of incidence and sound frequency. Attempts to interpret these data led to the conclusion that the observed data had undergone a transformation or distortion of some kind.

Simple, parallel-rod targets were studied in an effort to obtain reverberation patterns whose form could be predicted theoretically. The striking differences between the calculated and observed patterns were interpreted as being caused by a moiré effect, of a type not previously reported in the literature. An optical superpositon of the calculated reverberation pattern and the raster of plotter lines by which the acoustic pattern is displayed showed many of the features observed in the acoustic data.

The analytical theory of optical moiré pattern formation has been adapted to the acoustic case. Theoretically calculated moiré patterns for double-rod and multiple-rod targets are shown to agree closely with the observed patterns. A method of extending the work to the more difficult cases of reverberation from plane and corrugated sheets is indicated.

[redacted] [redacted] [redacted]

TABLE OF CONTENTS

Page

LIST OF TABLES

LIST OF FIGURES

LIST OF SYMBOLS

		Units
a	radius of plane piston	m
c_L	longitudinal (compressional) wave velocity	$m.sec^{-1}$
c_T	transverse (rotational) wave velocity	$m.sec^{-1}$
d	rod separation	m
h	integer	-
k	wavelength constant	m^{-1}
L	plate thickness	m
m	indexing parameter for moiré fringes	-
n	indexing parameter for diffraction maxima	-
n	order of interference	-
r	indexing parameter for raster lines	-
R	slope of raster lines	deg.sec
U	group velocity	$m.sec^{-1}$
α_t	sound power transmission coefficient	-
$\langle \Delta\theta \rangle$	mean raster line separation	deg
θ	angle of incidence	deg
θ_o	θ intercept for raster line r = 0	deg
λ	wavelength	m
λ	Lamé constant	$N.m^{-2}$
μ	Lamé constant	$N.m^{-2}$

		Units
ν	frequency	$sec.^{-1}$
ρ	density	$kg.m^{-3}$
ϕ	half angular beam width for transducer	deg

ACKNOWLEDGEMENTS

I wish to express my gratitude to Walter Barss for his supervision of this project.

I am also indebted to Ben Manning, without whose technical expertise and assistance the work could not have been successfully completed.

My special thanks must go to Krysha Derbyshire, who in addition to typing the manuscript, provided succour and encouragement throughout the duration of the project.

Financial support from the Defence Research Board of Canada is gratefully acknowledged.

CHAPTER 1

INTRODUCTION

1.1 Introduction to the Study

The problems encountered in the transmission of sound under the Arctic sea-ice canopy are a subject of continuing interest in underwater acoustics. The ability of nuclear submarines to navigate for extended periods under the ice has placed new emphasis on a complete understanding of the interaction of sonar navigating signals with an overlying ice sheet (Lyon, 1961). Acoustic waves are the only type of radiation suitable for the transmission of information under water over ranges greater than a few meters. Long range propagation utilises multiple reflections from the ice, and thus depends on the local interaction of sound rays with the ice-water interface. The research reported here is concerned with some details of this interaction, and in particular, with the techniques by which it may be studied in the laboratory.

1.2 Survey of Relevant Literature

The temperature and salinity of ice-covered sea water are usually such as to produce a sound velocity gradient which increases monotonically with depth (Marsh and Mellen, 1963). Under this condition, a sound ray, initially propagating at a small angle to the horizontal, will be continuously refracted towards the surface, and reflected downwards on encountering

the water-ice interface. Propagation over considerable distances is possible by alternate upward refraction and downward reflection. Figure 1.2.1 shows a typical velocity gradient and some possible ray paths.

The efficiency of propagation depends on the condition of the ice cover, as discussed by Milne (1967); the rougher the undersurface, the greater is the fraction of energy scattered away from the direction for specular reflection. Mellen and Marsh (1963) have correlated the rate of signal attenuation to the root mean square interface roughness. When a significant amount of the incident acoustic energy returns towards its source, the effect is termed reverberation. It sets the limit of detection on active sonar and echo navigating equipment.

There is some uncertainty concerning the dependence of reverberation on frequency and angle of incidence of sound on the ice layer (Chapman and Scott, 1966; Kutschale, 1969). Mellen and Marsh (1963) have measured ice reverberation levels as much as 40 dB above those predicted on the basis of reflection or scattering from the rough interface. One possible explanation of these results is that sound is not simply surface-reflected, but enters the body of the ice-sheet, and exists as elastic waves of various types. These waves dissipate energy by re-radiation into the water. Under certain conditions, some of this energy may be radiated in the direction of the source from which it came. Sasaki (1963)

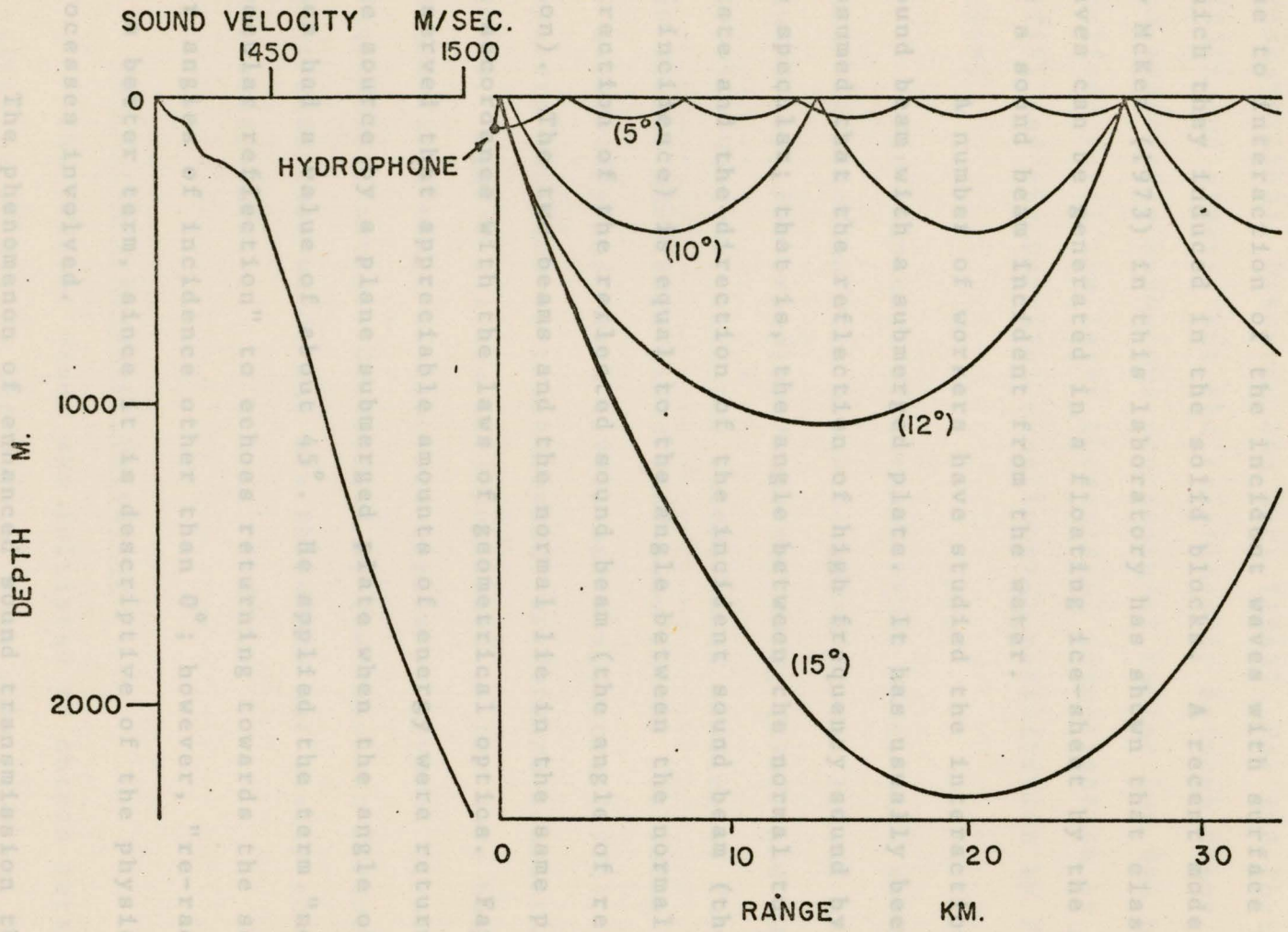

Figure 1.2.1. TYPICAL VELOCITY GRADIENT AND RAY PATHS IN THE ARCTIC OCEAN (after MILNE, 1967). SURFACE GRAZING ANGLES SHOWN IN BRACKETS.

studied reverberation (he termed it back-reflection) from metal blocks, many wavelengths thick, and deduced that it was due to interaction of the incident waves with surface waves which they induced in the solid blocks. A recent model study by McKee (1973) in this laboratory has shown that elastic waves can be generated in a floating ice-sheet by the action of a sound beam incident from the water.

A number of workers have studied the interaction of a sound beam with a submerged plate. It has usually been assumed that the reflection of high frequency sound by a plate is specular; that is, the angle between the normal to the plate and the direction of the incident sound beam (the angle of incidence) is equal to the angle between the normal and the direction of the reflected sound beam (the angle of reflection). The two beams and the normal lie in the same plane, in accordance with the laws of geometrical optics. Fay (1946) observed that appreciable amounts of energy were returned to the source by a plane submerged plate when the angle of incidence had a value of about 45°. He applied the term "non-specular reflection" to echoes returning towards the source for angles of incidence other than 0°; however, "re-radiation" is a better term, since it is descriptive of the physical processes involved.

The phenomenon of enhanced sound transmission through a submerged plate at certain discrete angles of incidence was first reported by Pierce (1936). Similarly, high ratios of

transmitted to received sound energy at well defined discrete angles have been reported by Sanders (1939), Smythe and Lindsay (1944), Osbourne and Hart (1945), Fay and Fortier (1951) and others, but the relationship between these effects and apparently anomalous non-specular reflection was not realised until the later theoretical investigation by Fay (1948) and the parallel experimental verification by Finney (1948).

The existence of several types of elastic wave, and their interaction with acoustic waves in the liquid have been studied by, for example, Press and Ewing (1951) and Hunkins (1960). However, with the exception of studies by Fay, Finney, and Sasaki mentioned above and some recent schlieren studies by Baborovsky and Marsh (1971) and Dragonette (1972), the emphasis has been on transmission or forward scattering from plates. Almost all the data published so far have been obtained for a range of discrete angles at several discrete frequencies, usually determined by the resonant frequency of the transducers used, and are therefore not easily compared with other data.

1.3 The Current Research Objective

The present study was initiated to obtain data from a selection of plates and models, both submerged and floating, over a large range of frequencies and angles of incidence.

A laboratory scale study was chosen, since it facilitated control of the maximum number of parameters. The floating ice layer was modelled by means of Plexiglas[1], glass and other plates suspended vertically in a water tank but provided with a pressure-release backing so as to simulate the acoustic conditions of a floating sheet. Means were available to vary the angle of incidence and the signal frequency continuously and simultaneously, and to obtain a chart of reverberation intensity over any specified range of either or both of these parameters.

The major portion of this thesis describes the data acquisition system, and the interpretation of data obtained. A curious effect, which is introduced by the frequency scanning detector, results in the partial or even complete suppression of the expected patterns in the reverberation charts under some conditions. The resulting modified patterns have been shown to be analogous to the moiré patterns familiar in optics, but produced in this case by the interaction of the acoustic reverberation pattern with the scanning pattern of the detector-plotter combination. The reverberation pattern produced by the target plate can be obtained by optically or mathematically "subtracting" the scanning pattern from the moiré pattern. Some simple examples are discussed, as are methods for the numerical solution of more complicated cases.

---

[1] Rohm and Haas Company of Canada Ltd., West Hill, Ontario.

CHAPTER 2

DESCRIPTION OF THE MODEL

2.1 The Medium

The experiments were conducted in a cylindrical water tank which had a diameter of 2.45 m and a water depth of 2.21 m. The tank was filled with water from the city supply, the level being maintained by a ball valve. The surface was kept clean by a skimmer and drain arrangement similar to the type used on domestic swimming pools. A small continuous overflow removed dust and floating debris. The water was chlorinted and filtered at regular intervals to inhibit the growth of algae and promote clarity. Fresh water was used, rather than sea water, for convenience of handling, and to take advantage of its lower attenuation coefficient. It also reduced corrosion problems with various metal fittings, which were made almost entirely of brass. A correction for the difference between the sound velocity in fresh and sea water could be applied where necessary.

2.2 Choice of an Ice Analogue

Since the investigation was to be at room temperature, it was necessary to use a material having similar acoustic properties to ice, but with a considerably higher melting point. The material chosen had to be available in homogeneous

plane sheets of a reasonable size, and various thicknesses. The acoustic parameters characterising an isotropic solid are the density ρ and the two Lamé constants μ and λ, or quantities derived from them. A parameter often used in studies of sound reflection from, or transmission through, a medium is the specific acoustic impedance, ρc, the product of density and the appropriate sound velocity, c. This product, also known as the characteristic impedance, has greater significance as a characteristic property of the medium than either ρ or c individually, and is analogous to the index of refraction in optics. An isotropic elastic solid can support two types of bulk elastic wave; the longitudinal or compressional wave with velocity c_L, and the transverse or rotational wave with velocity c_T; giving rise to two values of ρc. The following expressions have been derived in the literature for the velocities in terms of the Lamé constants:-

$$c_L = \sqrt{\frac{\lambda + 2\mu}{\rho}} \qquad (2.1)$$

$$c_T = \sqrt{\frac{\mu}{\rho}} \qquad (2.2)$$

A survey of the published properties of common engineering solids revealed that the most promising ice analogues

were among the considerable number of glasses and plastics available commercially. Figure 2.2.1 shows in diagrammatic form the transverse and longitudinal velocities of the materials investigated, compared with the sound velocities in ice and water. Figure 2.2.2 presents a similar treatment for the values of ρc. It was decided to use Plexiglas, whose values of ρc were closest to those of ice. The only disadvantage was that it had a transverse wave velocity smaller than the velocity of sound in water. This implied that no critical angle could exist for transverse waves in Plexiglas immersed in water, whereas such an angle did exist in ice. The critical angle is predicted by Snell's Law, occurring when the angle of incidence of sound at the interface of two dissimilar materials is such that the angle of refraction is 90°. At angles of incidence equal to or greater than the critical angle no sound is transmitted into the second medium. A similar effect in optics is known as total internal reflection. Some work was also done on plate glass, which exhibits no such effects, but whose impedance values are about four times larger.

An ideal ice analogue for the purposes of the current study would be a plastic material of lower density than Plexiglas, but having greater tensile strength; a combination of properties that would result in a larger value of c_T, but would maintain the value of ρc_T near that of ice. Several new types of plastic, both pre-formed sheets and casting resins, have been examined in the laboratory as they became

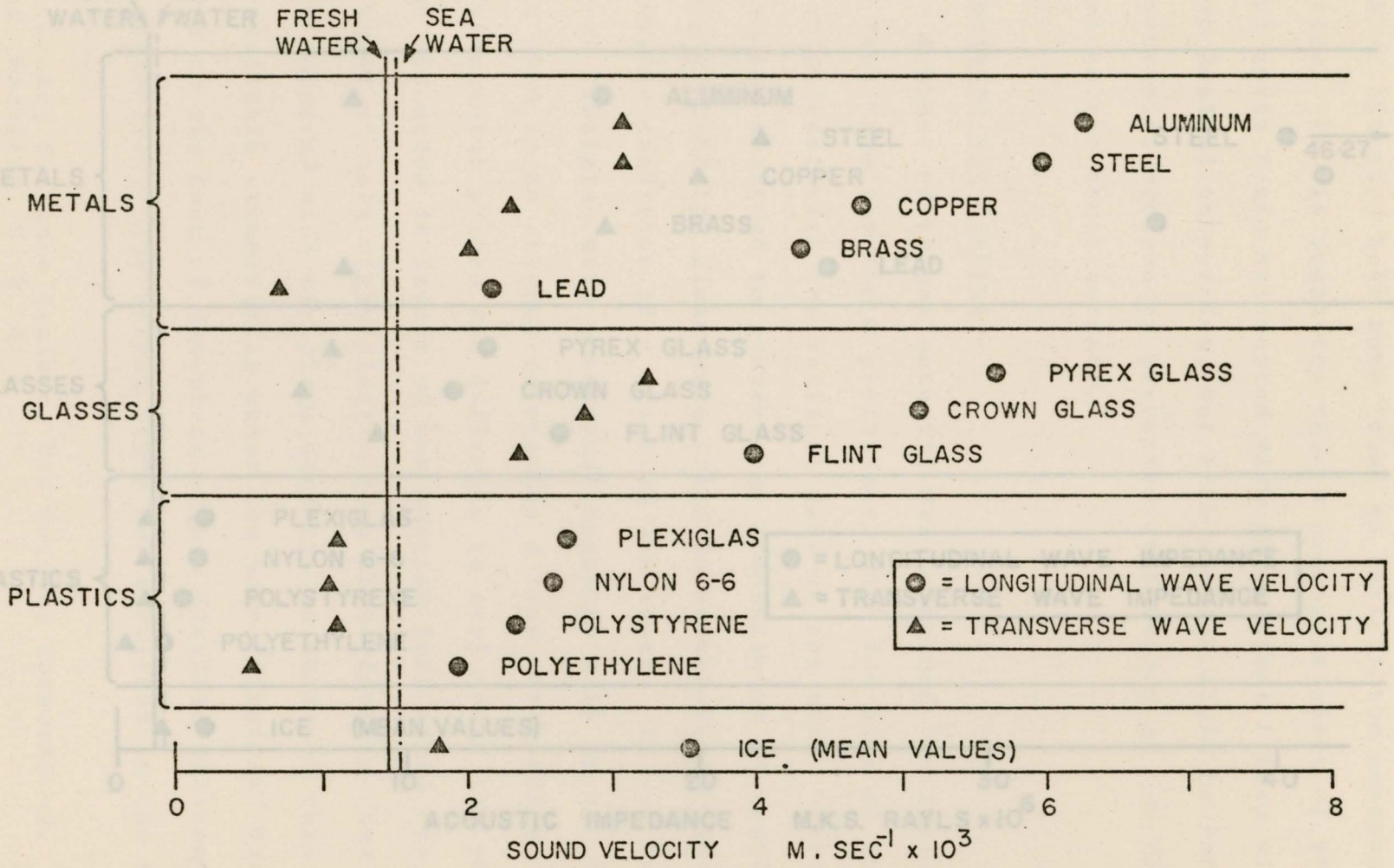

Figure 2.2.1. SOUND VELOCITIES IN SOLIDS, FRESH WATER AND SEA WATER

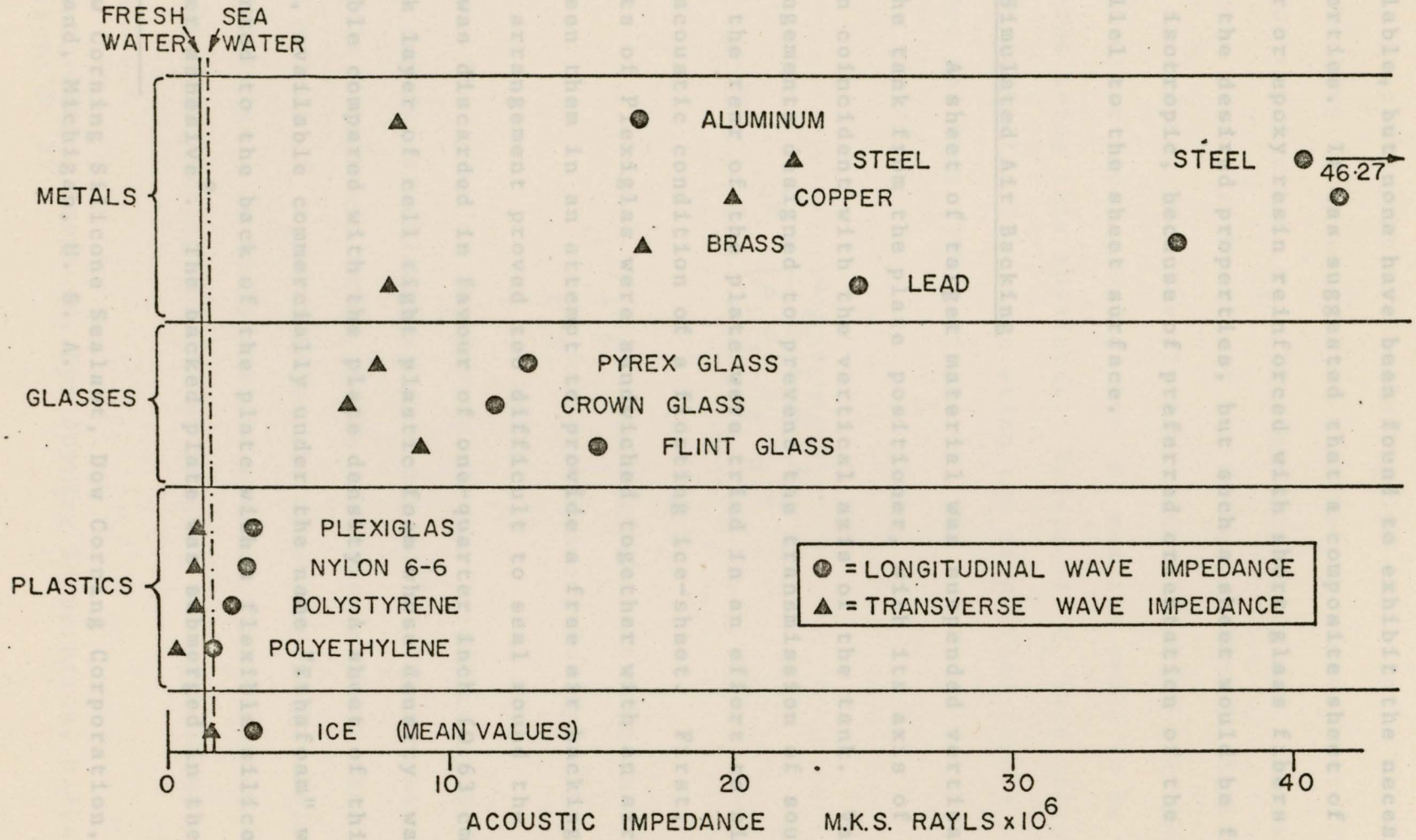

Figure 2.2.2. ACOUSTIC IMPEDANCE OF SOLIDS, FRESH WATER AND SEA WATER

available, but none have been found to exhibit the necessary properties. It was suggested that a composite sheet of polyester or epoxy resin reinforced with short glass fibers might give the desired properties, but such a sheet would be far from isotropic, because of preferred orientation of the fibers parallel to the sheet surface.

2.3 Simulated Air Backing

A sheet of target material was suspended vertically in the tank from the plate positioner, with its axis of rotation coincident with the vertical axis of the tank. Various arrangements designed to prevent the transmission of sound from the rear of the plate were tried in an effort to simulate the acoustic condition of a floating ice-sheet. First, two sheets of Plexiglas were sandwiched together with an air space between them in an attempt to provide a free air backing. This arrangement proved too difficult to seal round the edges, and was discarded in favour of one-quarter inch (0.63 cm) thick layer of cell tight plastic foam whose density was negligible compared with the plate density. A sheet of this foam, available commercially under the name "Ethafoam" was cemented to the back of the plate with a flexible silicone rubber adhesive[2]. The backed plate was submerged in the tank

---

[2] Dow Corning Silicone Sealant, Dow Corning Corporation, Midland, Michigan, U. S. A.

with a transducer acoustically coupled directly to the Ethafoam backing in an attempt to measure its sound power transmission coefficient α_t. The coupling agent was a smear of silicone grease[3]. No signal was detected above background by this transducer when the plate was insonified by a transmitter on the other side, showing that α_t was too small to be measured using this apparatus. Values of α_t were calculated for an air-solid interface using the simplified theory of Kinsler and Frey (1962) p. 131 :-

$$\alpha_t = \frac{4 \rho_1 c_1 \rho_2 c_2}{(\rho_1 c_1 + \rho_2 c_2)^2} \qquad (2.3)$$

where $\rho_1 c_1$ = specific acoustic impedance of air

$\rho_2 c_2$ = specific acoustic impedance of solid

The value of α_t for an air-ice interface is 5.6×10^{-4}, and for air-Plexiglas is 5.0×10^{-4}. Electrical and acoustic background noise in the instruments meant that such small values of α_t were below the measurement threshold of the apparatus. It was therefore assumed that Ethafoam was a suitable air backing for the purpose of the experiment.

---

[3] Dow Corning 4 Compound, Dow Corning Corporation, Midland, Michigan, U. S. A.

2.4 Pulse Considerations

No attempt was made to treat the walls of the tank with sound absorbing materials, so it was necessary to use a pulsed measuring technique to enable the desired reflection or echo to be distinguished from undesired ones off the tank wall, etc. A pulsed source also reduced the possibility of setting up standing wave patterns in the water. Short, constant-amplitude trains of acoustic waves, known as tone-bursts, were projected into the tank from a transducer fixed in the tank wall, and were received by a receiving transducer clamped in a mount adjacent to the transmitter. For convenience, tone-bursts about 1 millisecond long were usually used, during which time a wavefront travelled 1.48 m in water. The shortest path for a desired reflection was 2.32 m, allowing the transmitted and received signals to be easily distinguished when displayed simultaneously on a double-beam oscilloscope. Finney (1948), working at a frequency of 32 kHz, showed that a tone-burst impinging on a submerged plate produced steady conditions in less than 0.1 millisecond. Since this experiment was performed under similar conditions, no correction for transient conditions was needed.

2.5 Scaling Factor

The frequency, ν , of the incident tone-burst was continuously variable between 100 kHz and 1 MHz, giving a range of wavelengths in water of 1.48 cm to 0.15 cm. Most

naval sonar systems operate on a fixed frequency in the range 3 to 40 kHz (Horton, 1965), corresponding to wavelengths in sea water of 51 cm to 3.8 cm. Thus the scaling factor for the model dimensions ranged from 2.5 to 333. Plate thicknesses up to 2.5 cm were used, representing a scaled ice thickness up to 8 m.

A product often used in acoustics is the kL product where $k = 2\pi\nu/c$ and is termed the wavelength constant, and L is the plate thickness. For this experiment the range of values of kL is from 1.2 to 49.5, whereas values of kL calculated for field conditions are between 6.5 and 300, based on the ice thickness figures quoted by Mellen and Marsh (1963). The model was thus consistent with conditions met when a sonar transducer is operated in an ocean covered with a layer of ice whose thickness is such that $kL \leqslant 50$.

2.6 Criticism of the Model

It must be pointed out that this model is an extreme simplification of even the least complicated sea-ice system. Natural ice provides a far from simple interface with water, and is not isotropic. Pounder (1965), Langleben (1970) and others have shown that growing sea ice forms as a series of brine cells with vertical axes, growing downward from the ice surface. The growing layer rejects salt, so that a salt-rich layer exists beneath the ice, and at freezing temperatures forms a mushy semi-solid interface several centimeters thick.

This layer has sound transmission properties intermediate between those of ice and water, and at some frequencies could increase the transmission of sound between water and the ice cover. A further complication is the large number of air bubbles frozen into the ice, since air is released from solution as the water temperature drops. These can drastically alter the attenuation coefficient of the ice.

The stresses to which the formed ice sheet is subjected cause large numbers of cracks and surface irregularities. As the ice is compressed laterally it can buckle upwards and eventually break, allowing one edge to ride up, or "raft", over the other, so forming a composite sheet which is rapidly frozen together. Surveys of the Arctic region by submarine have shown even first year ice to be made up of a number of layers or floes rafted over one another. Such a structure is likely to have different acoustic and mechanical properties from a sheet of comparable thickness formed as one layer.

CHAPTER 3

THE SIGNAL PROCESSING AND DISPLAY SYSTEM

3.1 An Overview

The incident tone-bursts were obtained from a modified commercial waveform generator (see Appendix A) by applying a train of short rectangular pulses to its gate control input, at a repetition rate of 10 to 20 per second, and a sawtooth or ramp signal to its frequency control input, with a frequency sweep period of typically 30 to 40 seconds. The duration of the tone-bursts was much less than the sweep period, allowing each one to be treated as a burst of constant frequency waves. The resulting tone-bursts were amplified and fed, via an impedance matching transformer, to the transmitting transducer.

The reverberation signals were received by another transducer and fed to the gated receiver through two low noise preamplifiers and a calibrated step attenuator. Noise and spurious signals were rejected by the receiver circuits, allowing only echoes having the expected frequency and time of travel to be detected. The signal thus selected was then rectified, amplified and used to control the amplitude of a 10 Hz sine wave "wobble" generator, whose output voltage was thus determined by the strength of the reverberation signal. The wobble amplitude could be set to zero for a signal level

corresponding to the background noise, and would increase in response to larger signals. It was possible also to control the output contrast, i.e. the rate of increase of wobble amplitude with respect to signal level, in order to vary the range of signal strength that could be displayed visually, or otherwise recorded.

The output wobble signal was displayed as a function of angle of incidence θ, and frequency ν, on a modified X - Y chart recorder. The X displacement was proportional to the change in frequency, and the Y displacement was proportional to the slowly varying angle of incidence. The rates of change of θ and ν were adjusted to give about one or two degrees per frequency sweep. The output chart was built up as a series of parallel lines, slightly inclined to the axis, in much the same way as a television picture is built up one line at a time by a raster scan. Where a reverberation signal was present the wobble amplitude increased the effective width of the scan line in response to the signal strength. An example of a typical recorded pattern (for transmission rather than reverberation) is shown in Figure 3.1.1. Zero degrees on the chart corresponds to normal incidence of the tone-bursts on the target plate.

A block diagram of the electronics is shown in Figure 3.1.2, and a photograph in Figure 3.1.3. Detailed descriptions of individual units are not included in this thesis

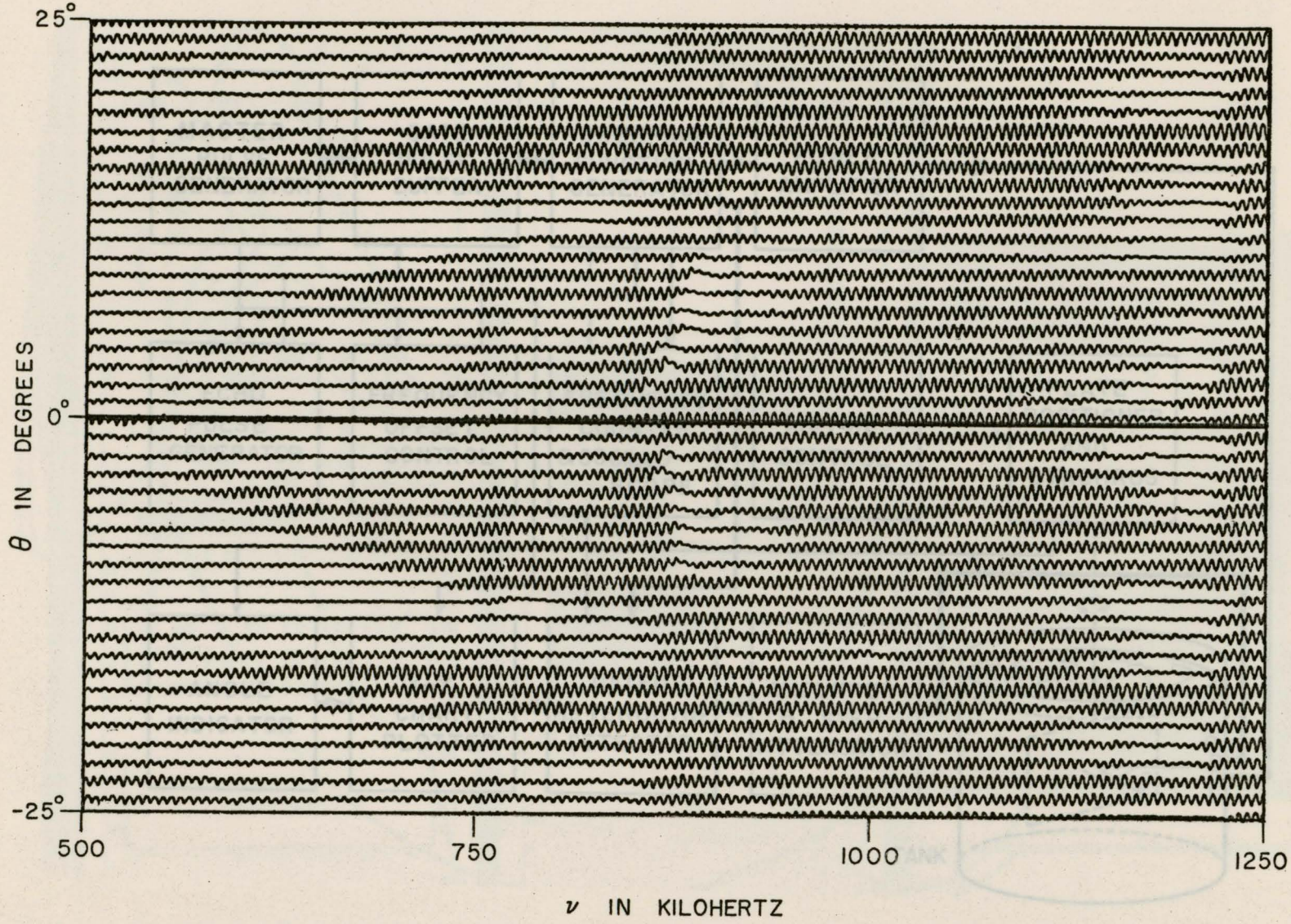

Figure 3.1.1. EXAMPLE OF PLOTTER OUTPUT : TRANSMISSION PATTERN FROM PLATE GLASS 0·63 CM THICK

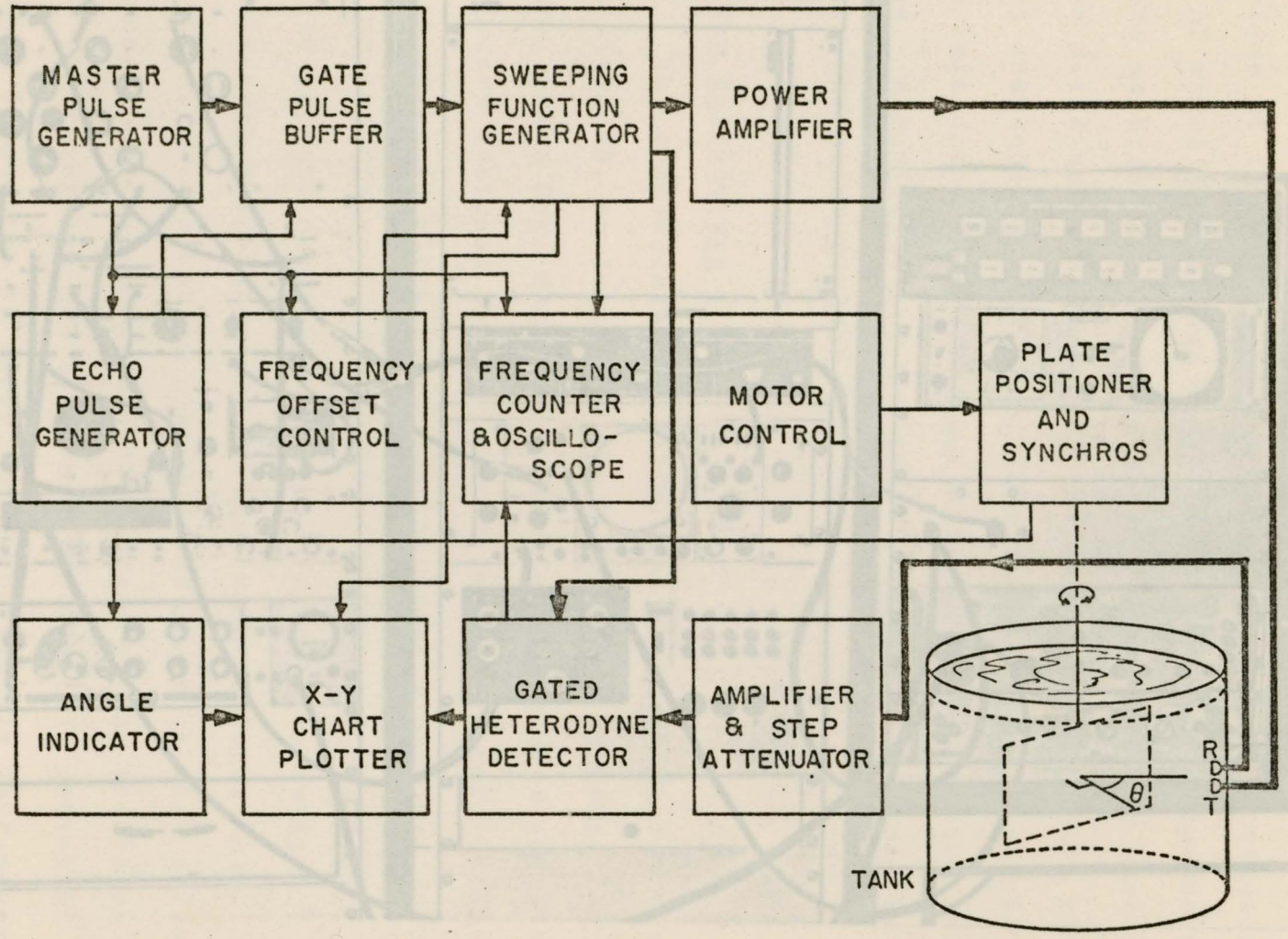

Figure 3.1.2. BLOCK DIAGRAM OF ELECTRONICS : PRINCIPAL SIGNAL PATHS SHOWN AS HEAVY LINES

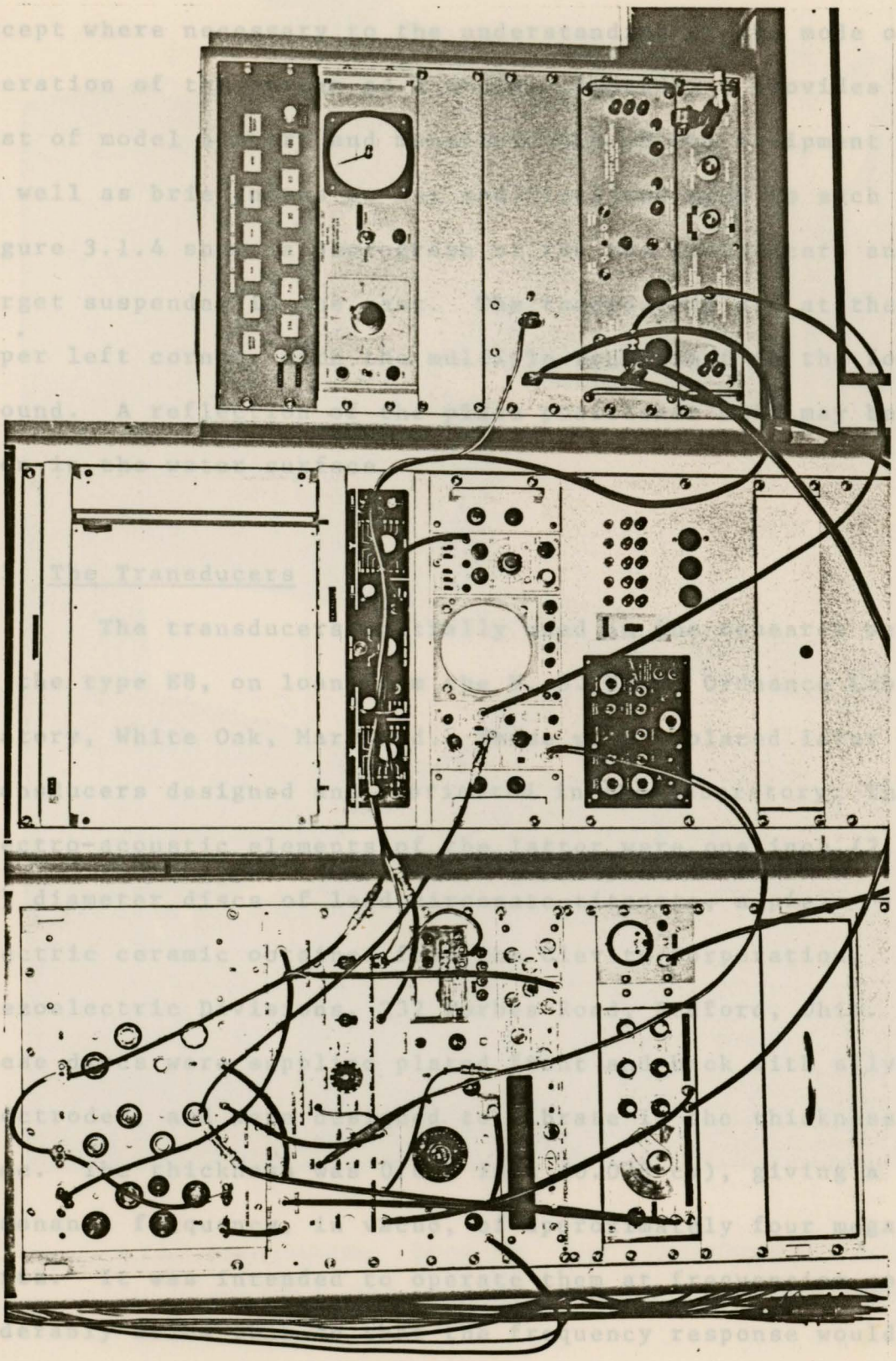

Figure 3.1.3. PHOTOGRAPH SHOWING THE ELECTRONIC APPARATUS

except where necessary to the understanding of the mode of operation of the system as a whole. Appendix A provides a list of model numbers and manufacturers of the equipment used, as well as brief notes on any modifications made to each unit. Figure 3.1.4 shows a photograph of the two transducers and a target suspended in the tank. The transducers are at the upper left corner, with the multiple rod target in the foreground. A reflection of the plate positioner unit may be seen in the water surface.

3.2 The Transducers

The transducers initially used in the research were of the type E8, on loan from the U. S. Naval Ordnance Laboratory, White Oak, Maryland. These were replaced later by transducers designed and fabricated in the laboratory. The electro-acoustic elements of the latter were one inch (2.54 cm) diameter discs of lead zirconate-titanate, a piezoelectric ceramic obtained from the Clevite Corporation, Piezoelectric Divisions, 232 Forbes Road, Bedford, Ohio. These discs were supplied plated front and back with silver electrodes, and were designed to vibrate in the thickness mode. The thickness was 0.015 inch (0.038 cm), giving a resonance frequency, in vacuo, of approximately four megahertz. It was intended to operate them at frequencies considerably below this so that the frequency response would be fairly flat.

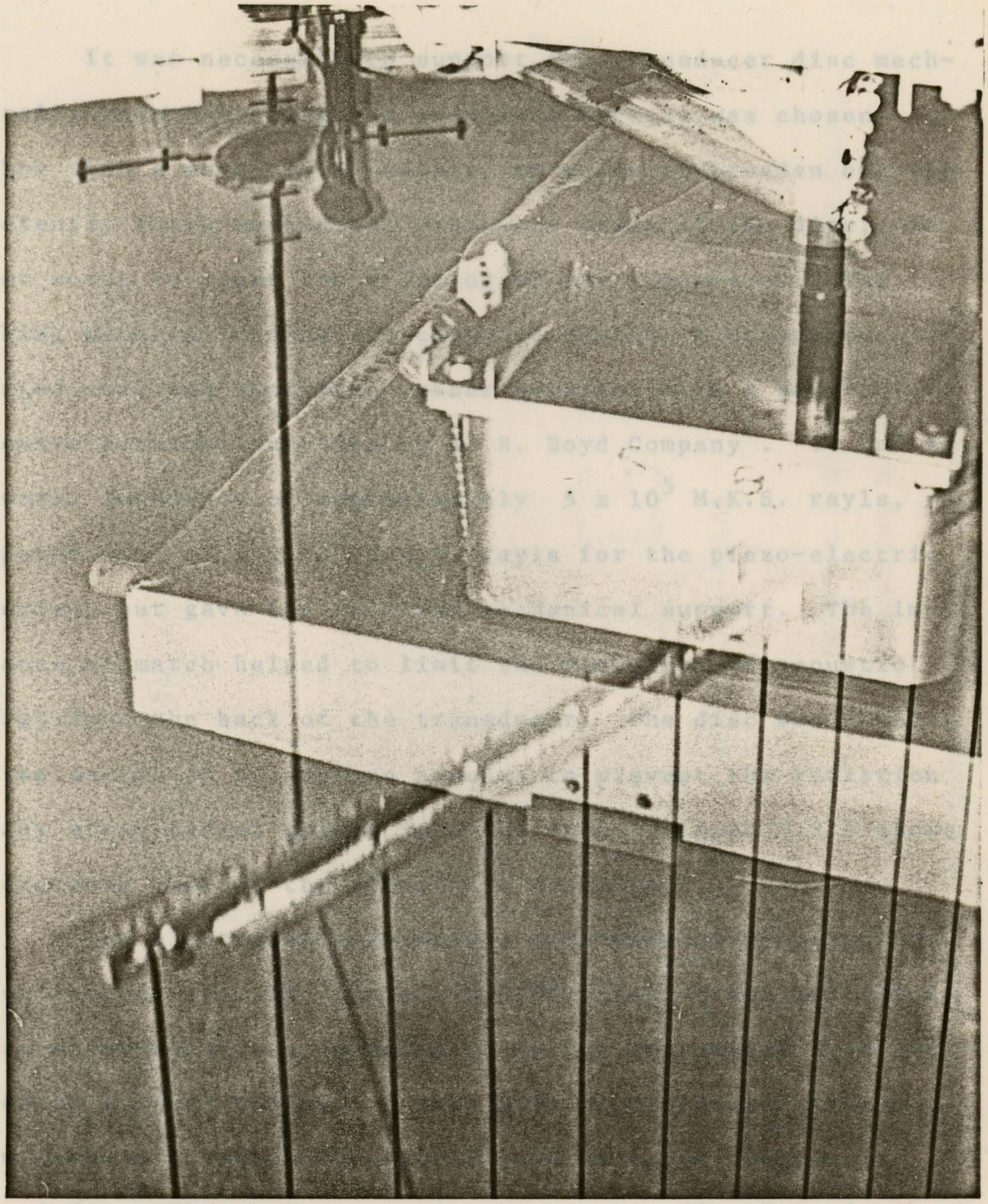

Figure 3.1.4. PHOTOGRAPH SHOWING THE TRANSDUCERS AND A MULTIPLE ROD TARGET SUSPENDED IN THE TANK

It was necessary to support the transducer disc mechanically when vibrating. A compliant backing was chosen rather than a more rigid support, in order to broaden out the inherently sharp mechanical resonance peaks of the disc; in other words to lower the Q-factor of the transducer. The backing material chosen was corprene DK-153, a composite sponged cork and synthetic rubber material with a self-adhesive backing, supplied by A. B. Boyd Company[4]. It had an acoustic impedance of approximately 5×10^5 M.K.S. rayls, compared with 2.3×10^7 M.K.S. rayls for the piezo-electric material, but gave the required mechanical support. The impedance mismatch helped to limit the radiation of acoustic energy from the back of the transducer. The disc was mounted in the centre of a corprene annulus to prevent the radiation of any stray radial energy into the tank. Figure 3.2.1 shows an exploded view of the transducer assembly.

The electrical connections were made by pressing the front face of the disc against a 0.002 inch (0.005 cm) thick brass sheet which was soldered on to the transducer face and acted as a sound window. A thin film of dielectric grease (Dow Corning 4 Compound) ensured good acoustic coupling to the window. The rear connection was a thin circular piece of brass held in contact with the disc by pressure from a

---

[4] A. B. Boyd Company, 8033 N.E. Holman Street, Portland, Oregon, U. S. A.

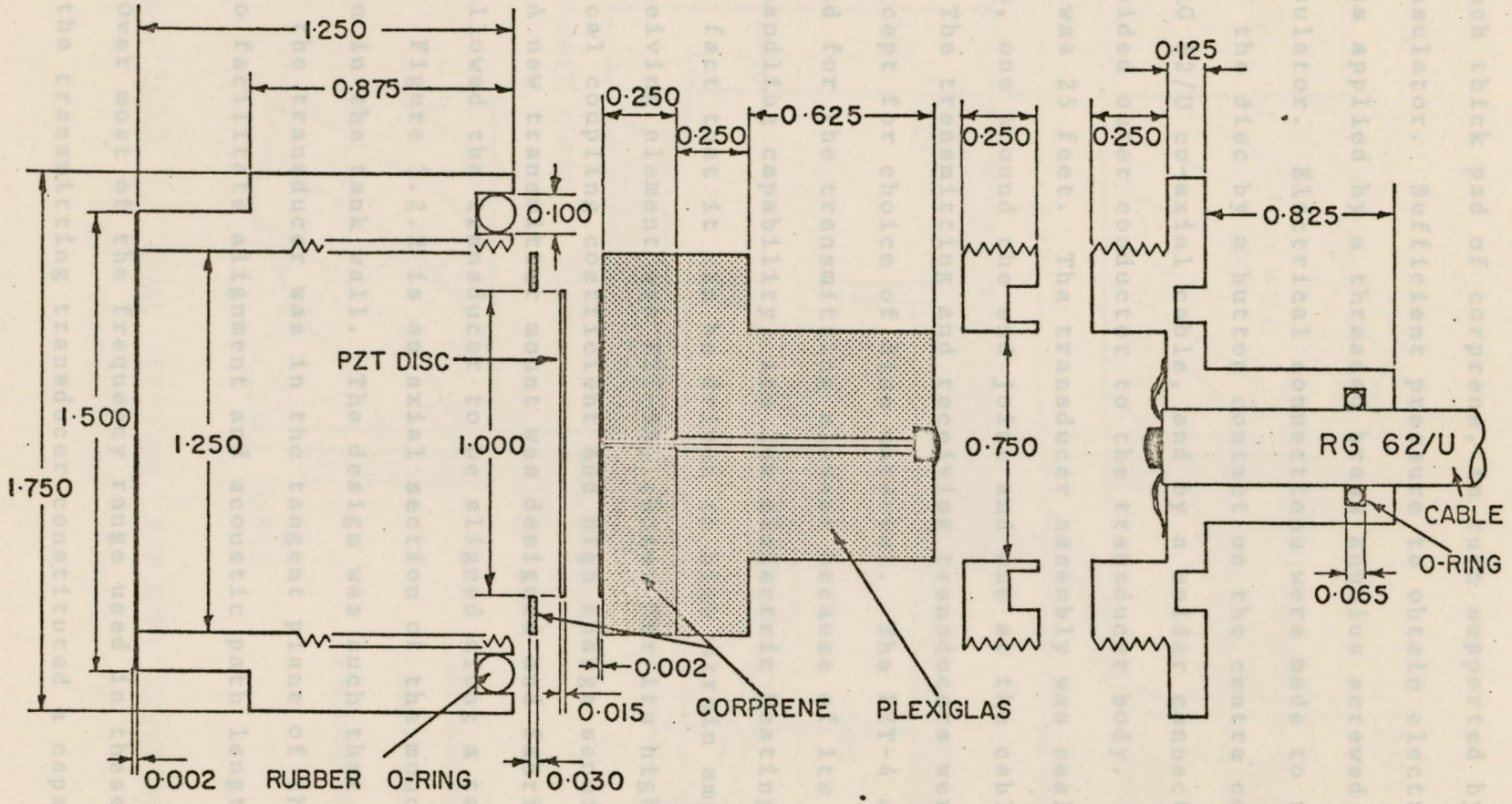

MATERIAL IS BRASS EXCEPT WHERE STATED

DIMENSIONS IN INCHES

Figure 3.2.1. AXIAL SECTION OF TRANSDUCER ASSEMBLY, EXPLODED VIEW

0.25 inch thick pad of corprene, in turn supported by a Plexiglas insulator. Sufficient pressure to obtain electrical contact was applied by a threaded brass annulus screwed in behind the insulator. Electrical connections were made to the rear face of the disc by a button contact on the centre conductor of an RG 62/U co-axial cable, and by a solder connection from the braided outer conductor to the transducer body. The cable length was 25 feet. The transducer assembly was sealed by two O-rings, one around the end joint and one at the cable outlet.

The transmitting and receiving transducers were identical except for choice of disc material. The PZT-4 ceramic was used for the transmitting element because of its superior power handling capability, its low dielectric heating loss, and the fact that it can be driven to high strain amplitudes. The receiving element was PZT-5A, chosen for its high electromechanical coupling coefficient and high charge sensitivity.

A new transmitter mount was designed and fabricated, which allowed the transducer to be aligned along a tank diameter. Figure 3.2.2 is an axial section of the mount in position in the tank wall. The design was such that the front face of the transducer was in the tangent plane of the tank wall, to facilitate alignment and acoustic path length measurements.

Over most of the frequency range used in these experiments, the transmitting transducer constituted a capacitive

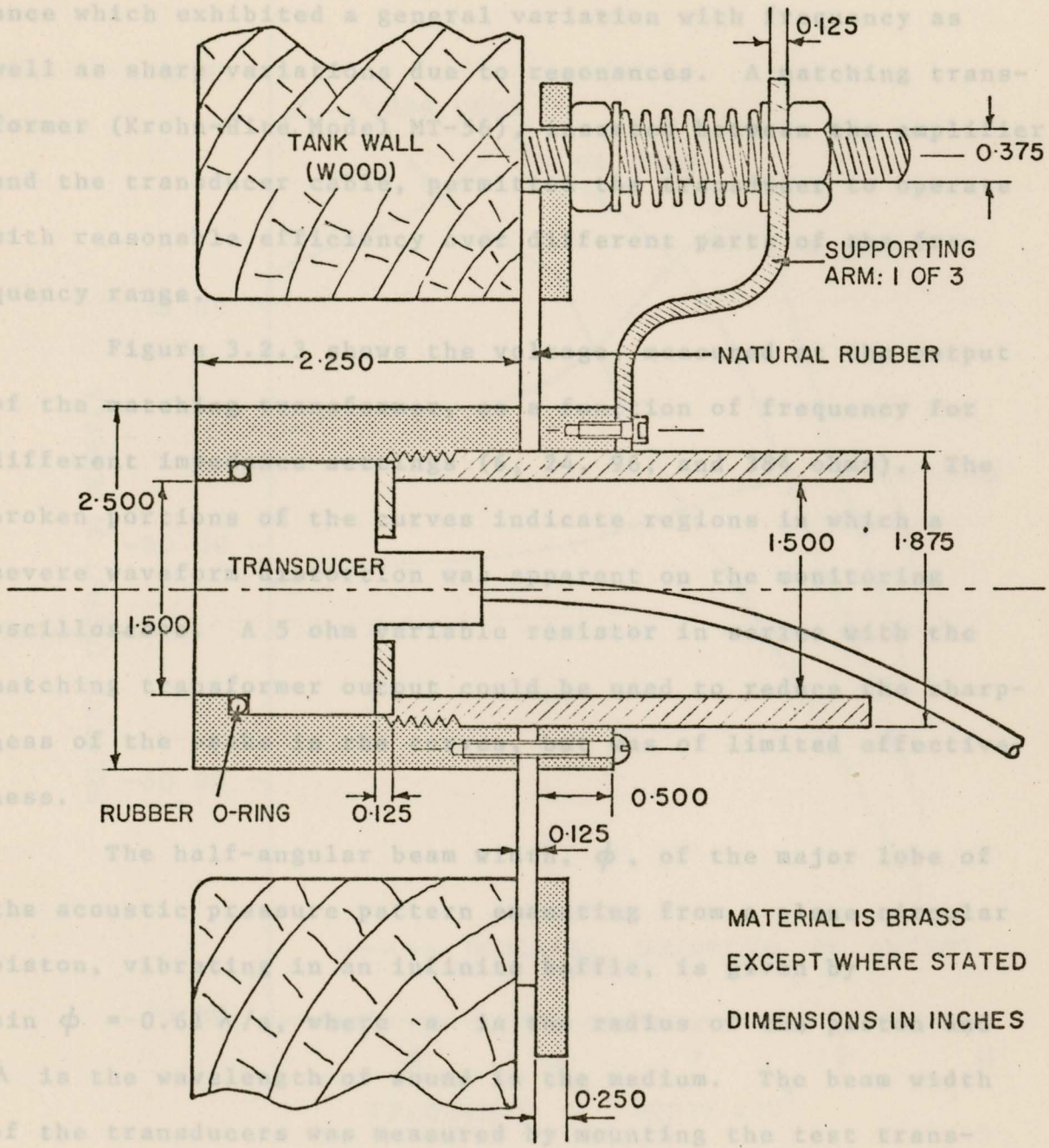

Figure 3.2.2. AXIAL SECTION THROUGH ADJUSTABLE MOUNT FOR TRANSMITTING TRANSDUCER

reactance and thus presented the amplifier with a load impedance which exhibited a general variation with frequency as well as sharp variations due to resonances. A matching transformer (Krohn-Hite Model MT-56), inserted between the amplifier and the transducer cable, permitted the transducer to operate with reasonable efficiency over different parts of the frequency range.

Figure 3.2.3 shows the voltage, measured at the output of the matching transformer, as a function of frequency for different impedance settings (6, 24, 96, and 384 ohms). The broken portions of the curves indicate regions in which a severe waveform distortion was apparent on the monitoring oscilloscope. A 5 ohm variable resistor in series with the matching transformer output could be used to reduce the sharpness of the peaks in the curves, but was of limited effectiveness.

The half-angular beam width, ϕ, of the major lobe of the acoustic pressure pattern emanating from a plane circular piston, vibrating in an infinite baffle, is given by $\sin \phi = 0.61 \lambda / a$, where a is the radius of the piston and λ is the wavelength of sound in the medium. The beam width of the transducers was measured by mounting the test transducer temporarily on the tank axis, exciting it with a continuous sine wave and rotating it at constant angular velocity by means of the plate positioner so that its transmitted

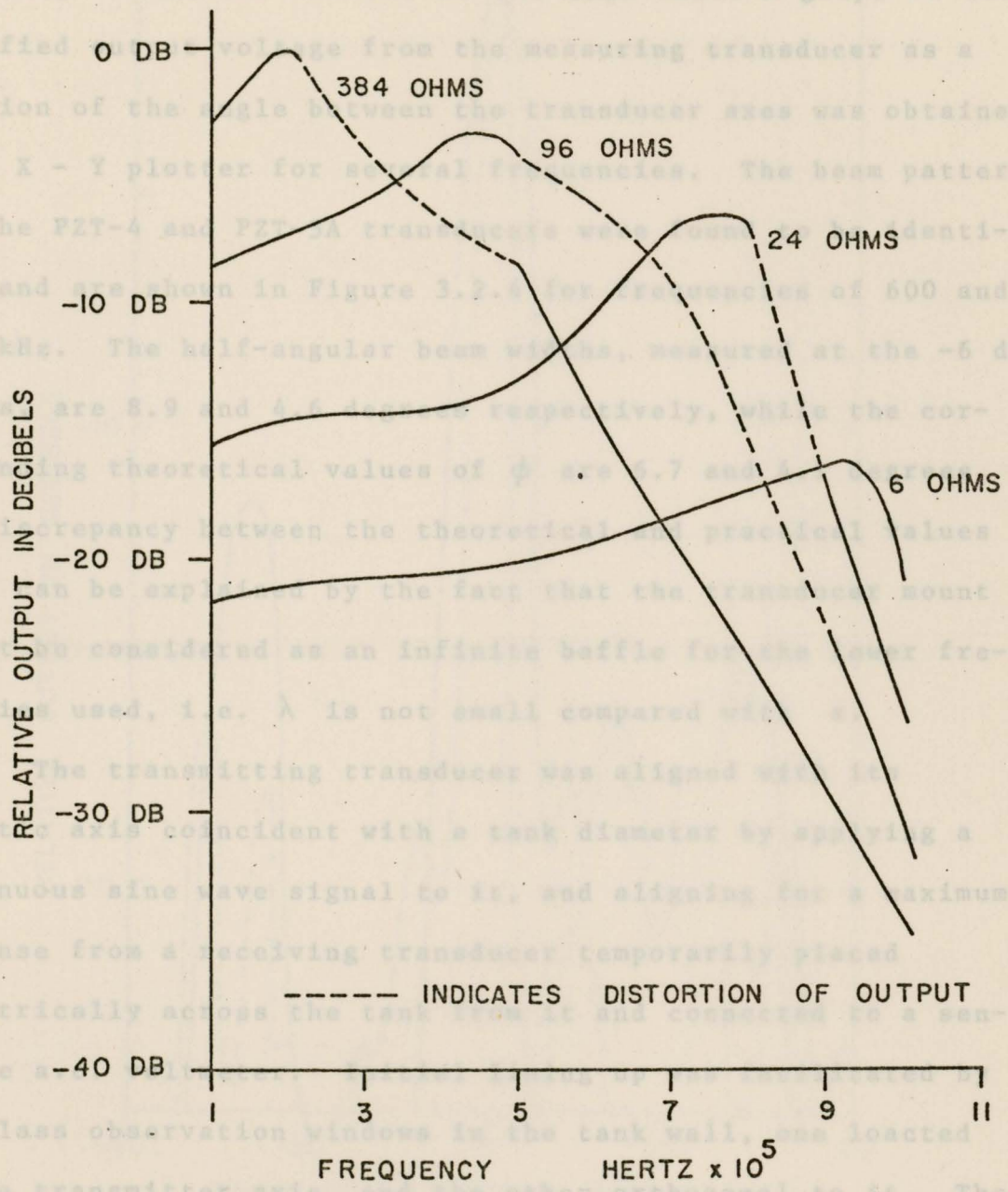

Figure 3.2.3 FREQUENCY RESPONSE OF TRANSMITTING TRANSDUCER USING DIFFERENT MATCHING IMPEDANCES

acoustic pressure pattern was swept across the face of a measuring transducer mounted in the tank wall. A graph of the rectified output voltage from the measuring transducer as a function of the angle between the transducer axes was obtained on an X - Y plotter for several frequencies. The beam patterns for the PZT-4 and PZT-5A transducers were found to be identical, and are shown in Figure 3.2.4 for frequencies of 600 and 1000 kHz. The half-angular beam widths, measured at the -6 dB points, are 8.9 and 4.6 degrees respectively, while the corresponding theoretical values of ϕ are 6.7 and 4.1 degrees. The discrepancy between the theoretical and practical values of ϕ can be explained by the fact that the transducer mount cannot be considered as an infinite baffle for the lower frequencies used, i.e. λ is not small compared with a.

The transmitting transducer was aligned with its acoustic axis coincident with a tank diameter by applying a continuous sine wave signal to it, and aligning for a maximum response from a receiving transducer temporarily placed diametrically across the tank from it and connected to a sensitive a.c. voltmeter. Initial lining up was facilitated by two glass observation windows in the tank wall, one loacted on the transmitter axis, and the other orthogonal to it. The receiving transducer was then clamped in an adjustable mount directly above the transmitting transducer, and aligned by allowing the incident sound beam to strike a plane reflector,

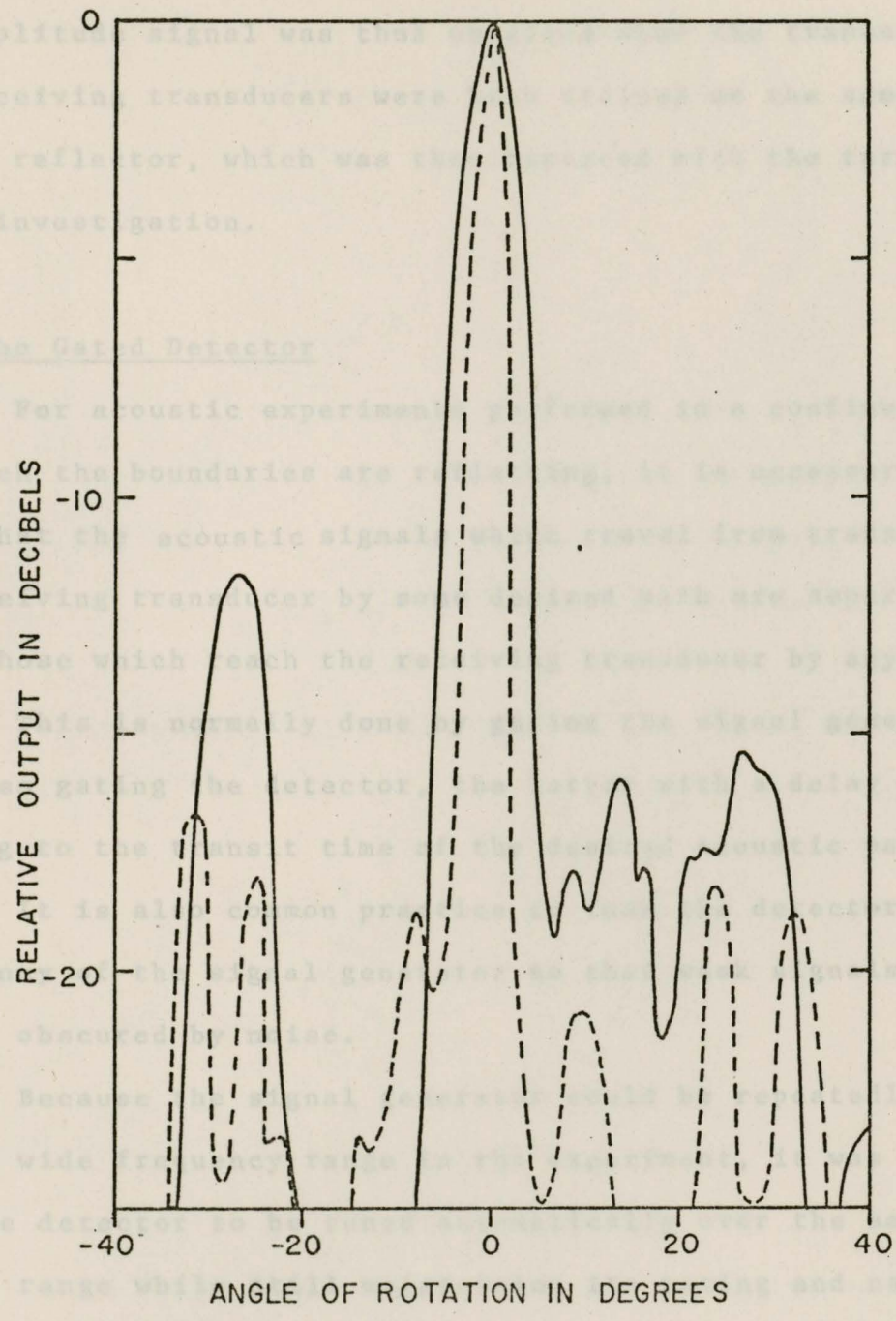

Figure 3.2.4. TRANSDUCER BEAM PATTERNS AT FREQUENCIES OF 600 KHZ (SOLID LINE) AND 1000 KHZ (BROKEN LINE)

positoned at the tank centre, at normal incidence. A maximum amplitude signal was thus obtained when the transmitting and receiving transducers were both trained on the same area of the reflector, which was then replaced with the target under investigation.

3.3 The Gated Detector

For acoustic experiments performed in a confined space, in which the boundaries are reflecting, it is necessary to ensure that the acoustic signals which travel from transmitting to receiving transducer by some desired path are separated from those which reach the receiving transducer by any other path. This is normally done by gating the signal generator and also gating the detector, the latter with a delay corresponding to the transit time of the desired acoustic path in the tank. It is also common practice to tune the detector to the frequency of the signal generator so that weak signals will not be obscured by noise.

Because the signal generator could be repeatedly swept over a wide frequency range in the experiment, it was necessary for the detector to be tuned automatically over the same frequency range while still maintaining its gating and narrow band-pass characteristics. A heterodyne system which provided both timimg and gating functions was developed in this laboratory, and was the subject of a Canadian patent granted to

Barss (1972). Its operation is as follows.

Tone-bursts and associated detector gating signals were generated by triggering a sweeping function generator (Data-Royal Waveform/Sweep Generator Type F230A) with timing signals initiated by a Tektronix Type 162 waveform generator, designated the Master Pulser. The leading edge of the rectangular master pulse triggered two Tektronix Type 161 pulse generators, each of which gave a delayed rectangular output pulse variable in delay, duration and amplitude. One of these, the Echo Pulser, was adjusted for a duration similar to the master pulse, and a delay time corresponding to the transit time of the desired reverberation signal in the tank. The master and echo pulses were added in the Gate Pulser Buffer (Figure 3.1.2) so that the Sweeping Function Generator was gated to produce a pair of tone-bursts, the second being delayed by a time equal to the transit time of the desired acoustic signal in the tank. The output of the second Type 161 pulse generator, applied to the frequency control input of the sweeping function generator, modified the frequency of the delayed echo tone-burst, the difference in frequency being determined by the amplitude of the delayed pulse. The tone-burst output from the generator was split: one part was amplified and drove the transmitting transducer through an impedance matching transformer, while the other part was applied to the mixer stage of the gated detector where the arrival of the electronically

delayed echo signal coincided with the arrival of the reverberation signal from the tank.

The acoustic reverberation signal from the tank was picked up by the receiving transducer, amplified by a low noise preamplifier, passed through a calibrated step attenuator and a second similar preamplifier and applied to the mixer stage of the gated detector. After some early work, it was found necessary to insert a high pass R-C filter between the two preamplifiers to eliminate 60 Hz hum. The reverberation signal was mixed with the frequency offset echo signal, which differed from it by a constant frequency difference, and the mixer output was amplified by a conventional, narrow-band transformer-tuned intermediate frequency (I. F.) amplifier. The I. F. transformers were tuned to 100kHz, and had a pass-band of only 1.90 kHz measured at the -6 dB points. The amplitude of the frequency offset pulse needed careful adjustment to ensure that the difference frequency was in the centre of the I. F. pass-band permitting the desired signal to be amplified and rectified in a voltage doubling diode circuit. The only signals which were present at the rectifier output were those which had the desired transit time and desired frequency, thus separating the reverberation signals from unwanted echoes and spurious noise. The rectifier output was filtered and integrated by a circuit which sustained the D.C. output of the integrator until reset to zero at the beginning of the next echo

pulse. A diagram of the timimg and typical amplitude of the various signals is shown in Figure 3.3.1 for a frequency giving strong reverberation.

The filtered output of the integrator was used to control the bias, and hence the gain, of a variable-gain pentode amplifier. This amplifier controlled the amplitude of a 10 Hz sine wave signal, generated by a built-in oscillator, in such a way that its amplitude was a function of the reverberation signal intensity. Controls were provided to vary the static bias and operating point of the pentode stage to provide peak limiting and dynamic range compression, allowing the contrast and sensitivity on the $\nu - \theta$ output charts to be controlled.

3.4 The Chart Plotter and Calibration

Output charts showing the reverberation intensity as a function of ν and θ were obtained from a modified Varian Model F80-AX-Y chart recorder. This was operated in the time-base mode, and adjusted so that the start of a frequency sweep commenced a pen traverse along the X - axis. At the end of the traverse the pen was automatically raised and returned to its starting point at high speed, ready for the next beginning-of-sweep signal.

The X traverse was calibrated in terms of frequency as follows. The frequency at the start of a sweep was read on a digital frequency counter, and in a typical case was 600 kHz. The chart was 14 inches long and a pen speed of 0.5 inch per

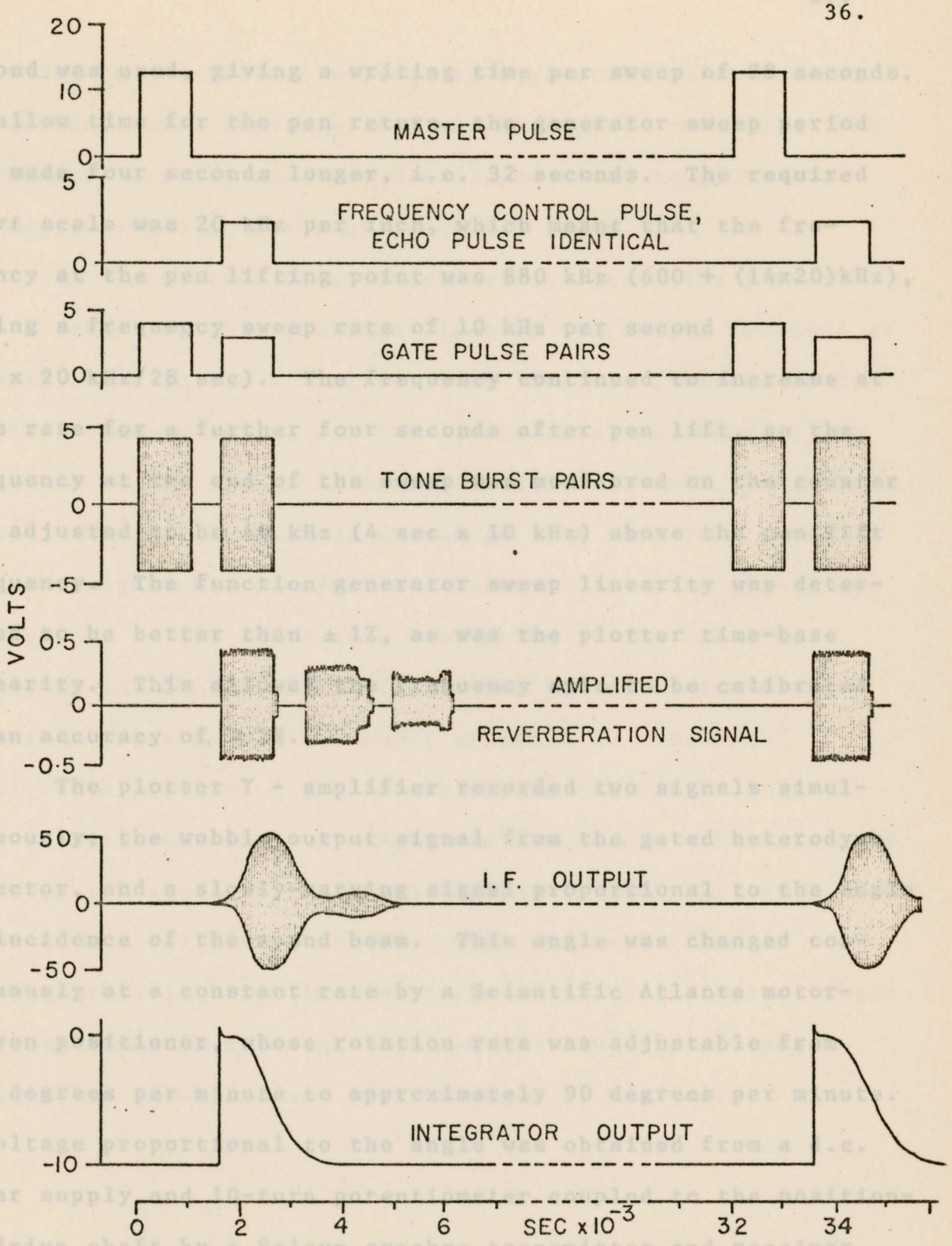

Figure 3.3.1. TIMING AND TYPICAL AMPLITUDE OF SIGNALS

second was used, giving a writing time per sweep of 28 seconds. To allow time for the pen return, the generator sweep period was made four seconds longer, i.e. 32 seconds. The required chart scale was 20 kHz per inch, which meant that the frequency at the pen lifting point was 880 kHz (600 + (14x20)kHz), giving a frequency sweep rate of 10 kHz per second (14 x 20 kHz/28 sec). The frequency continued to increase at this rate for a further four seconds after pen lift, so the frequency at the end of the sweep was monitored on the counter and adjusted to be 40 kHz (4 sec x 10 kHz) above the pen lift frequency. The function generator sweep linearity was determined to be better than ± 1%, as was the plotter time-base linearity. This allowed the frequency axis to be calibrated to an accuracy of ± 2%.

The plotter Y - amplifier recorded two signals simultaneously; the wobble output signal from the gated heterodyne detector, and a slowly-varying signal proportional to the angle of incidence of the sound beam. This angle was changed continuously at a constant rate by a Scientific Atlanta motor-driven positioner, whose rotation rate was adjustable from 0.5 degrees per minute to approximately 90 degrees per minute. A voltage proportional to the angle was obtained from a d.c. power supply and 10-turn potentiometer coupled to the positioner drive shaft by a Selsyn synchro transmitter and receiver. The chart Y - axis was calibrated at its end points by

switching in a reference voltage to bypass the potentiometer. The θ scale most commonly used was 10 degrees per inch. The positioner rotation rate was usually adjusted to give about one degree rotation for each frequency sweep.

In the absence of a reverberation signal the plotter drew a series of thin parallel lines on the chart, inclined at a small angle to the X - axis. Each line was produced by a single frequency sweep, and the line separation, $\langle \Delta\theta \rangle$, was a measure of the change in angle of incidence over the sweep period. When the angle and frequency were such that a reverberation signal was present, the intensity of that signal was represented on the chart as a broadening of the ink line, caused by the 10 Hz oscillation of the pen about its mean position. Thus each $\nu - \theta$ chart provided an immediate qualitative picture of the reverberation pattern of a target over a continuous range of angle and frequency. The frequency range of the apparatus was from 200 kHz to 2000 kHz, and continuous axial motion of the target was restricted to approximately 100° by limit switches in the positioner. These switches could be adjusted to allow the 100° arc of target position to encompass any desired angle of incidence.

CHAPTER 4

EXPERIMENTAL OBSERVATIONS OF REVERBERATION PATTERNS

4.1 Plane Plates

The targets studied initially were a glass plate 0.63 cm thick, and a Plexiglas plate 1.90 cm thick, both of which were airbacked. Sample $\nu - \theta$ charts are shown for these in Figures 4.1.1 and 4.1.2, of which the latter is a composite of charts for successive frequency ranges. These figures were cropped at $\theta = 40^{\circ}$, because no reverberation was observed for larger angles. It may be noted that Figure 4.1.1 covers only half of the angular range of Figure 4.1.2.

Both charts exhibit intensity variations which depend on frequency but not on angle. Such variations may be due in part to imperfect tracking of the two function generator frequencies during a sweep, but are mainly attributable to the non-uniform frequency characteristics of the transducers used. These two charts were obtained with different pairs of transducers and, as the angle-independent variations occurred at different frequencies, showed that the effect was primarily due to the transducer characteristics.

In view of this interpretation, Figure 4.1.1 can be described as having several dark streaks extending from about 800 to 1600 kHz and for angles from zero to about 30 degrees. The streaks are not smooth, but have a fine structure which in

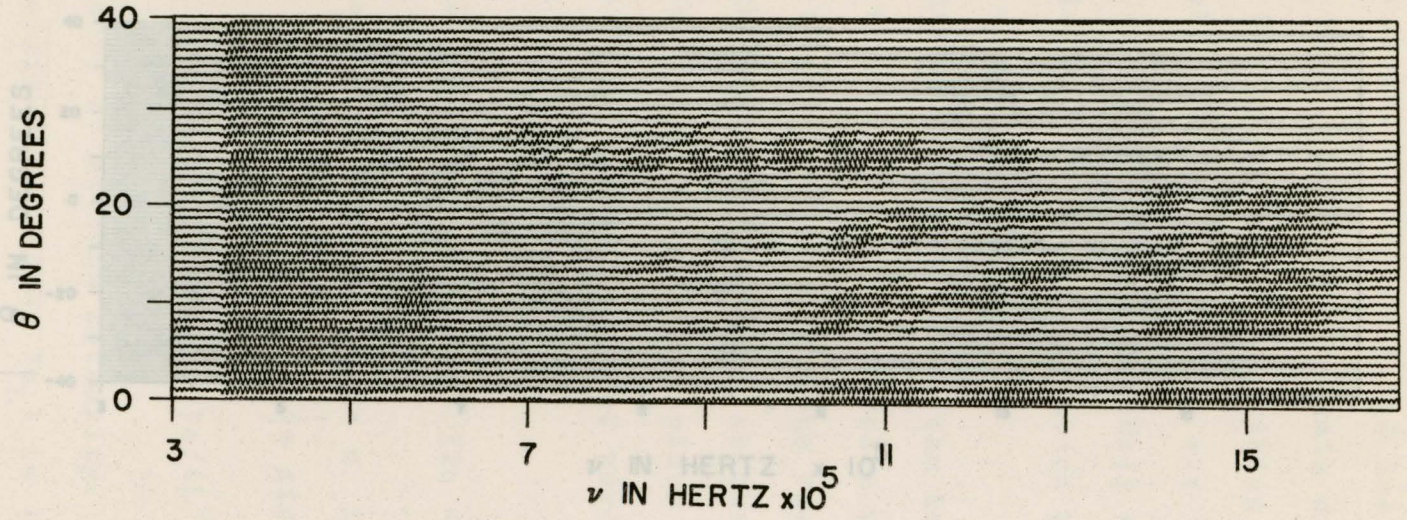

Figure 4.1.1. REVERBERATION FROM AIR-BACKED PLATE GLASS, THICKNESS 0·63 CM.

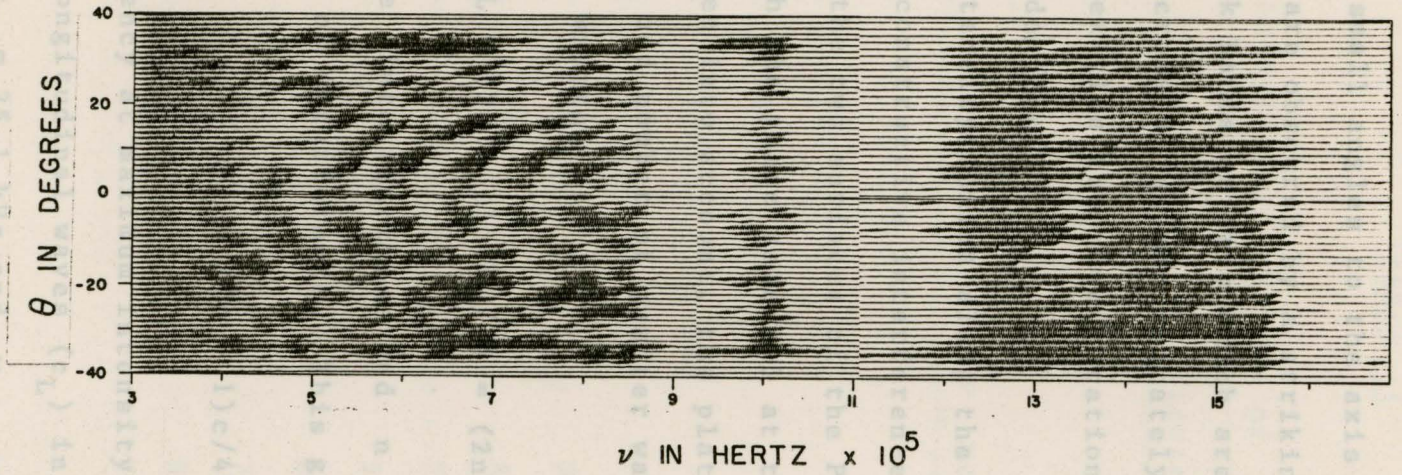

Figure 4.1.2. REVERBERATION FROM AIR-BACKED PLEXIGLAS, THICKNESS 1·91 CM.

some cases is regular enough to be referred to as ripples.

In contrast, if Figure 4.1.2 has any streaks inclined at similarly small angles to the axis of symmetry (θ = 0 degrees), they are obscured by a striking pattern of alternating light and dark bands or arcs which are quite symmetrical about the axis and cross it at approximately equal frequency intervals. For Plexiglas the reverberation pattern is observable to nearly 40 degrees.

The intensity maxima along the axis are readily explained as due to constructive interference between sound waves reflected from the two surfaces of the Plexiglas at normal incidence. With the phase reversal at the Plexiglas-water interface taken into account, the plate thickness must correspond to an odd number of quarter wavelengths. This condition may be written as

$$L = (2n - 1)\ \lambda / 4 = (2n - 1)\ c/4\nu \qquad (4.1)$$

where L is the plate thickness and n is an integer representing the order of interference. This gives

$$\nu_n = (2n - 1)c/4L \qquad (4.2)$$

for the frequency at maximum intensity. From Figure 2.2.1 the velocity of longitudinal waves (c_L) in Plexiglas is 2.67 km/sec, giving ν_1 = 35.1 kHz and $\nu_n - \nu_{n-1}$ = 70.2 kHz. Table 1 lists the calculated values of ν_n for $1 < n < 12$ against the measured values from Figure 4.1.2, determined from the

TABLE 1

Measured and Calculated Values of ν_n for Constructive Interference for Figure 4.1.2

n	ν_n calculated	ν_n measured	% difference
1	35.1 kHz	-	-
2	105	-	-
3	175	-	-
4	246	-	-
5	316	-	-
6	386	385 kHz	0.26
7	456	450	1.32
8	526	522	0.76
9	597	590	1.17
10	667	662	0.75
11	737	730	0.95
12	807	802	0.62

centre of each dark area. As can be seen the agreement is excellent, the difference being smaller than the uncertainty of frequency calibration in every case.

For angles other than normal incidence, one possible mode of energy transfer is by waveguide propagation. Acoustic energy incident from the water can enter the plate and propagate along it by multiple internal reflection at boundaries, as shown diagrammatically in Figure 4.1.3. This mode of propagation was discussed by Press and Ewing (1951) for the case of horizontally polarised shear waves (SH waves). After many reflections the amplitude will be greatest for those waves for which constructive interference occurs between the multiply reflected rays. The equation governing waveguide mode propagation is simply the mathematical statement of this condition. Referring to Figure 4.1.3 it is seen that if the wavefront at PT is to interfere constructively with coincident wavefront which has travelled the additional path PQRT, it is required that

$$\overline{PQRT} = 2L \cos\theta = n\lambda = nc/\nu \qquad (4.3)$$

where λ is the wavelength measured along the ray path. The group velocity U is given by $c \sin\theta$. The detector gate was open for sufficient time to accept guided waves which may have been reflected from the edge of the plate, and re-radiated into the water, except at angles of incidence so small that

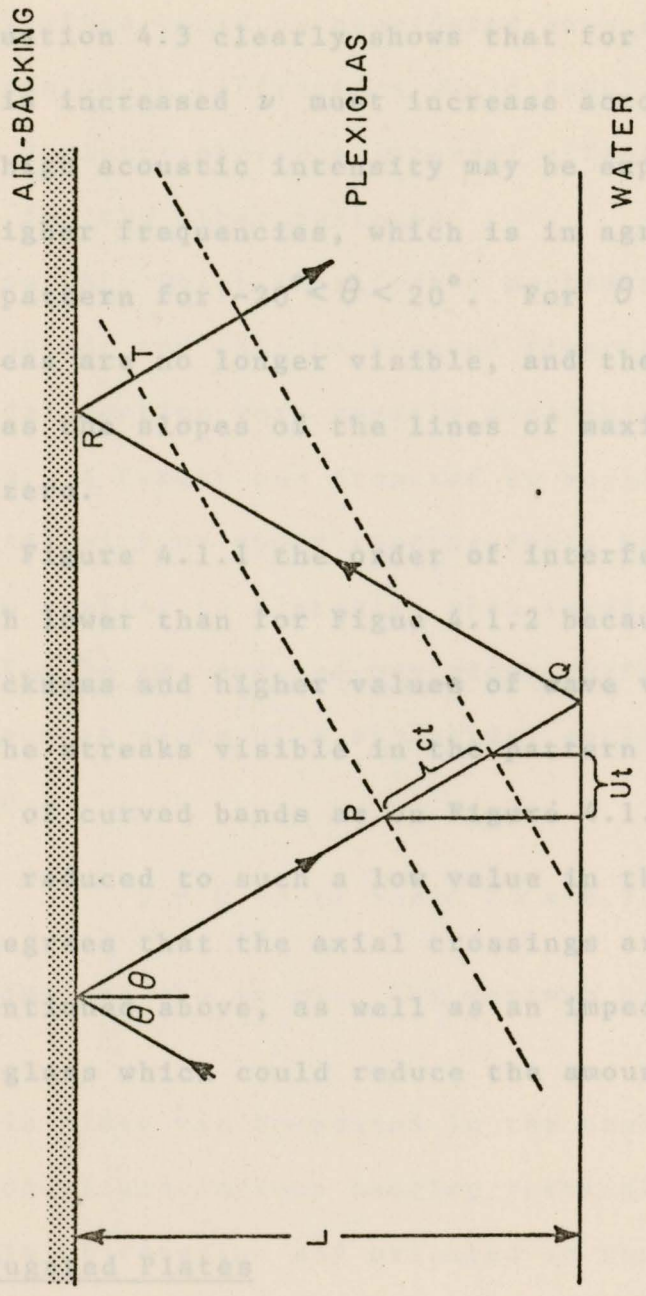

Figure 4.1.3. WAVEGUIDE PROPAGATION OF SOUND IN A PARALLEL SIDED PLATE

the group velocity was too low. It may be noted from Figure 4.1.2 that most of the curved bands are weak for $-5^\circ < \theta < 5^\circ$.

Equation 4.3 clearly shows that for a given value of n, as θ is increased ν must increase accordingly. Thus the areas of high acoustic intensity may be expected to be concave towards higher frequencies, which is in agreement with the observed pattern for $-20^\circ < \theta < 20^\circ$. For $\theta > 20^\circ$ the crescent shaped areas are no longer visible, and the pattern becomes confused as the slopes of the lines of maximum intensity approach zero.

In Figure 4.1.1 the order of interference was expected to be much lower than for Figue 4.1.2 because of the smaller plate thickness and higher values of wave velocity in the plate. The streaks visible in the pattern may be the off-axis ends of curved bands as on Figure 4.1.2, but with the intensity reduced to such a low value in the angular range below 8 degrees that the axial crossings are invisible for the reason mentioned above, as well as an impedance mismatch from water to glass which could reduce the amount energy in the plate.

4.2 Corrugated Plates

The weakness of the reverberation pattern for glass, and the confused pattern for larger angles and frequencies for Plexiglas, led to the thought that a plate with a periodic surface structure would yield a reverberation pattern whose

features could be attributable to direct reflections from the front surface, and explained in terms of its periodicity. The periodic surface could be considered as a diffraction grating, and a recognisable diffraction would result, with surface reflections dominant over the internal effects thought to be responsible for the other features.

A surface which facilitated mathematical description was a sinusoid; and thin corrugated fiber-glass panels having a sinusoidal section were readily available as translucent roofing panels. A target was prepared by building up one side of such a panel with an epoxy casting resin having acoustic properties similar to Plexiglas when cured. The finished target was 88 x 55 cm, and had one plane surface which was parallel to the mean plane of a sinusoidal surface described by the expression

$$y = 0.63\ (1 + \sin 2\pi x/6.72) \qquad (4.4)$$

where dimensions are in cm. The maximum plate thickness was 1.80 cm.

This plate was suspended in the tank with the crests of the sinusoidal undulations hanging vertically, i.e. parallel to the axis of rotation and oriented so that sound was incident on the sinusoidal face. A typical reverberation pattern, such as Figure 4.2.1 was very complicated, with no features which have been identified with certainty as due to the surface

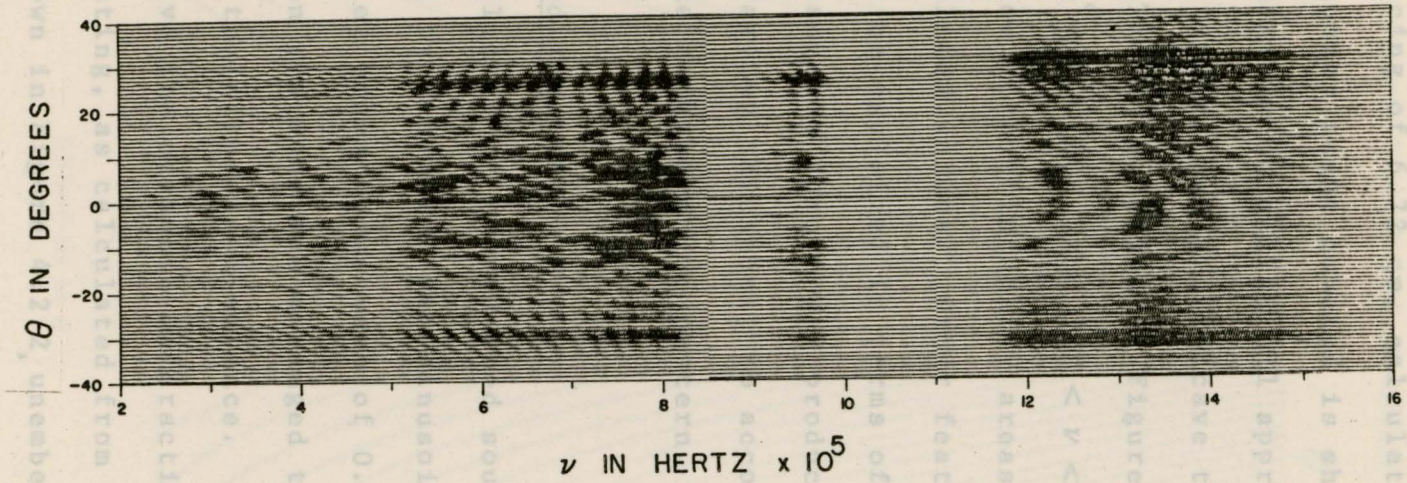

Figure 4.2.1. REVERBERATION FROM UNBACKED PLASTIC SHEET WITH REAR SURFACE PLANE AND FRONT SURFACE HAVING SINUSOIDAL CORRUGATIONS OF WAVELENGTH 6·72 CM.

configuration. The multiple slit optical diffraction pattern for a slit spacing of 6.72 cm, calculated for part of the angle and frequency range covered is shown in Figure 4.2.2. The lines of maximum intensity all approach the axis of symmetry asymptotically, and are concave towards high angles and frequencies. The only region of Figure 4.2.1 which has these features is $15^{\circ} < \theta < 30^{\circ}$, and $700 < \nu < 820$ kHz, and the spacing of these strong intensity areas does not correspond with the calculated values. Other features of the pattern could also not be explained in terms of the multiple slit model. No reasonable theory was produced, for a plate of periodically varying thickness, to account for any of the features of the reverberation pattern.

4.3 Simplified Targets

The reflected or re-radiated sound field in the tank was simplified by replacing the sinusoidal plate by a plane grid of parallel brass rods, each of 0.32 cm diameter. The spacing between the rods was arranged to be identical with the wavelength of the sinusoidal surface. In this way it was hoped to observe the acoustic diffraction pattern of a multiple slit grating, as calculated from the laws of geometrical optics and shown in Figure 4.2.2, unembellished by any spurious reflections from within the body of the target. The grid of rods was considered as a reflection grating, and since the

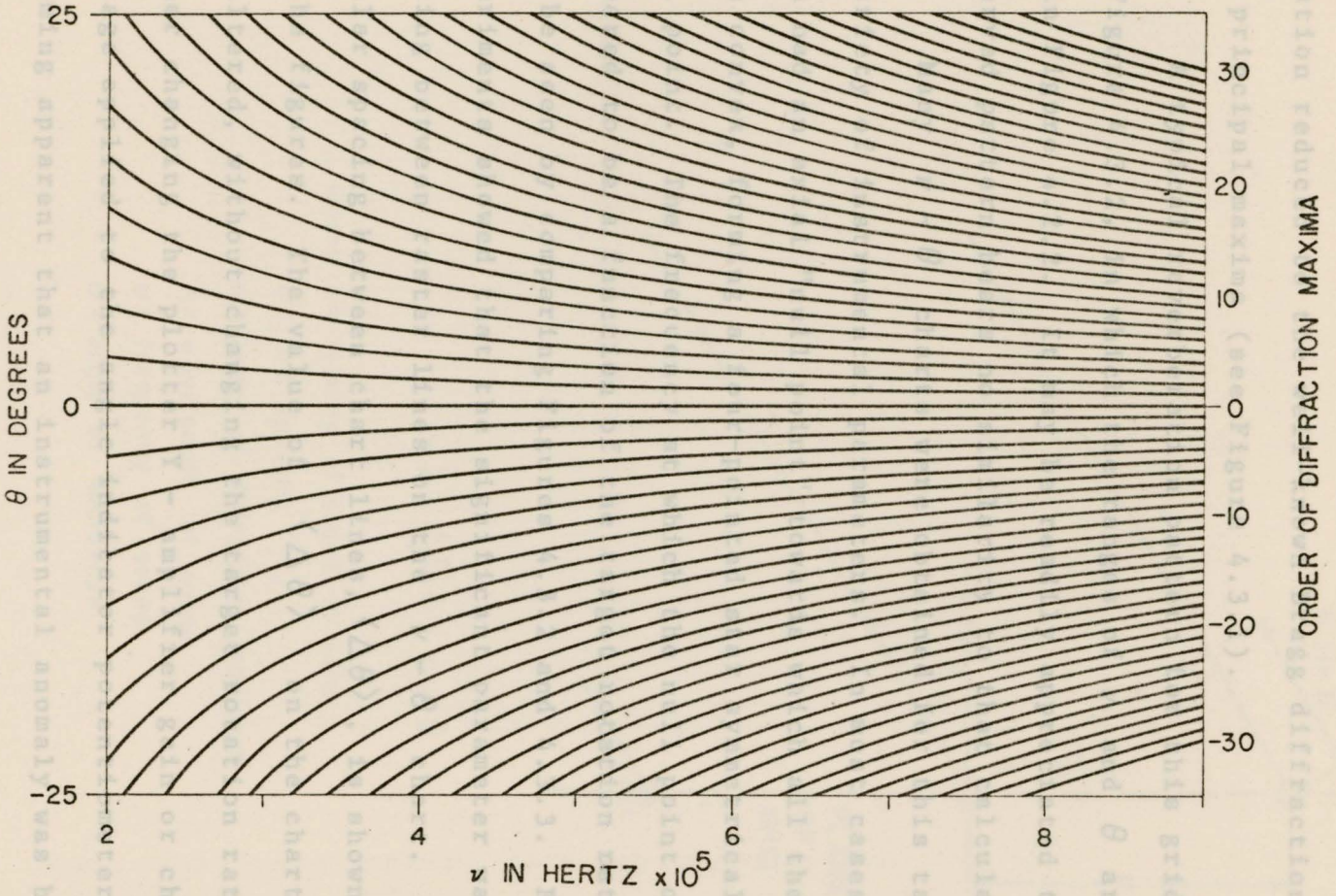

Figure 4.2.2. CALCULATED POSITION OF DIFFRACTION MAXIMA FOR GRID SPACING OF 6·72 CM.

angles of incidence and reflection were equal, the governing equation reduced to the well-known Bragg diffraction condition for principal maxima (see Figure 4.3.1).

A typical reverberation pattern for this grid is shown in Figure 4.3.2, in which the ranges of ν and θ are the same as in Figure 4.2.2. It may be readily appreciated that the observed pattern bears no similarity to that calculated.

Many $\nu - \theta$ charts were obtained for this target using a variety of instrumental parameters. In most cases the pattern had an axial "null point" towards which all the streaks were convex, forming a four-pointed star symmetrical about the null point. The frequency at which the null point occurred appeared to be a function of the target rotation rate, which may be seen by comparing Figures 4.3.2 and 4.3.3. Further experiments showed that the significant parameter was the spacing between raster lines on the $\nu - \theta$ chart. The mean angular spacing between chart lines, $\langle \Delta\theta \rangle$, is shown on each of the figures. The value of $\langle \Delta\theta \rangle$ on the charts could be altered, without changing the target rotation rate, by either changing the plotter Y - amplifier gain or changing the voltage applied to the angle indicator potentiometer. It was becoming apparent that an instrumental anomaly was being observed, since altering the raster spacing on the print-out device was unlikely to cause any changes in the acoustic field inside the tank.

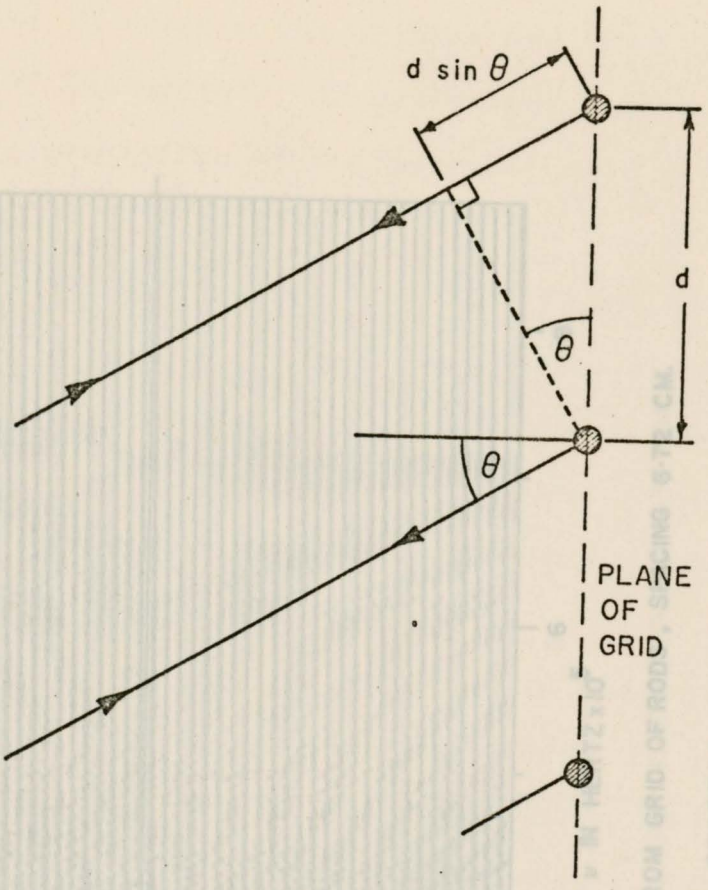

$$n\lambda = \frac{n\,c}{\nu} = 2\,d\sin\theta$$

where c = velocity of sound in water
d = rod spacing
n = order of diffraction maximum
λ = wavelength of sound
ν = frequency of sound
θ = angle of incidence

Figure 4.3.1. RAY DIAGRAM AND CONDITION FOR DIFFRACTION MAXIMA FOR A GRID OF PARALLEL RODS

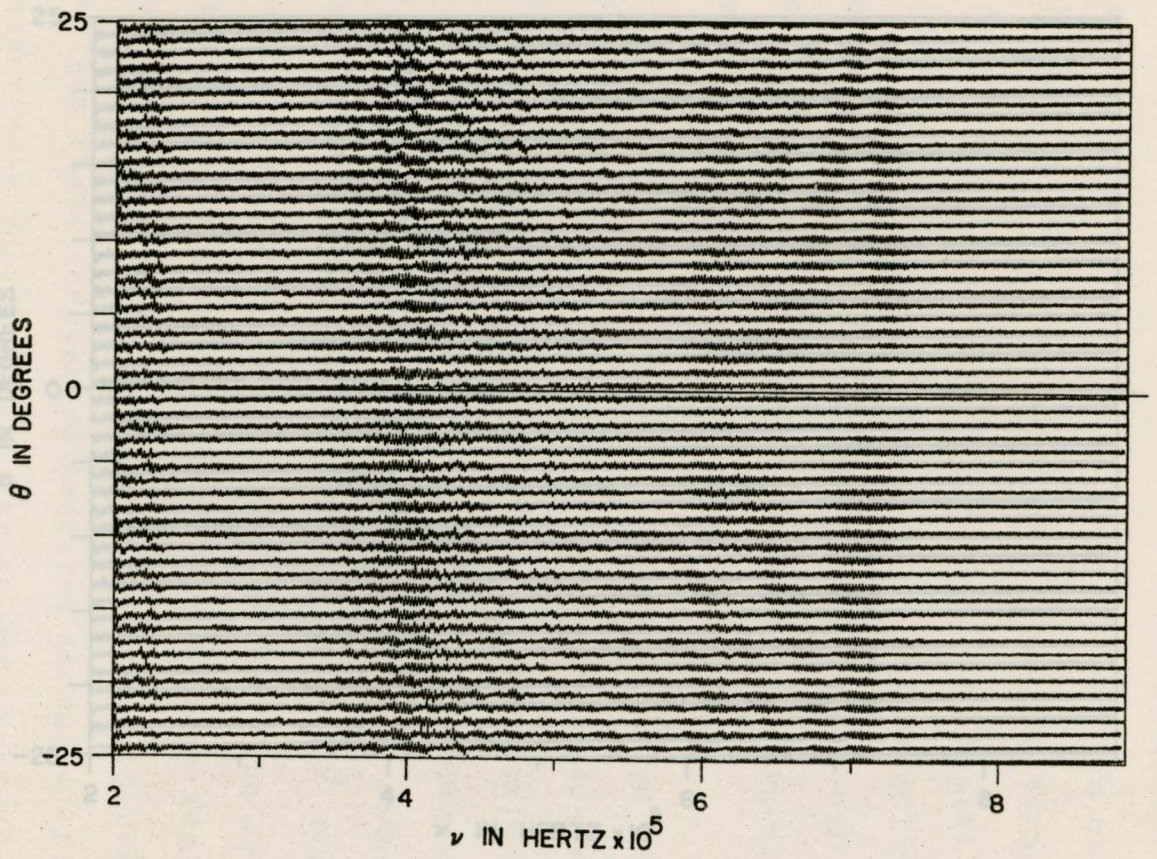

Figure 4.3.2. REVERBERATION FROM GRID OF RODS, SPACING 6·72 CM.

$\langle \Delta\theta \rangle$ = 0·91 DEGREES PER SWEEP

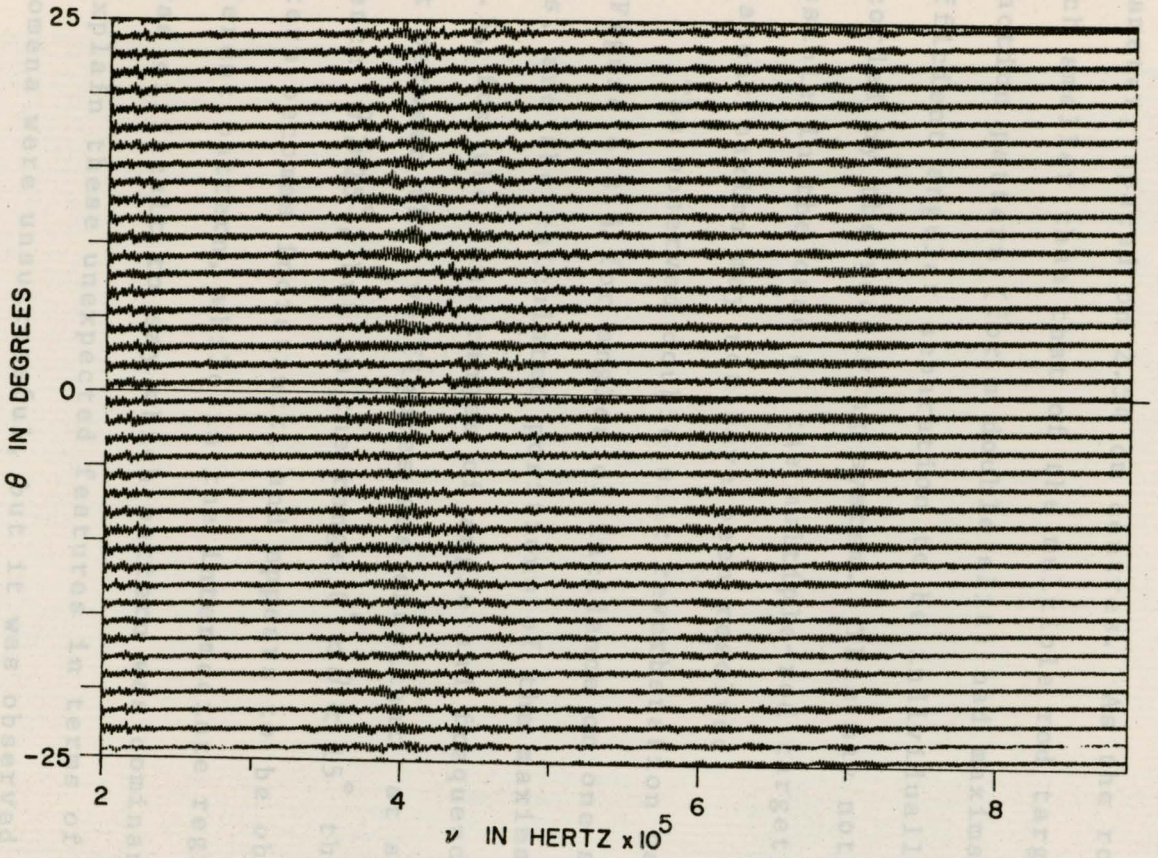

Figure 4.3.3. REVERBERATION FROM GRID OF RODS, SPACING 6·72 CM.

$\langle \Delta\theta \rangle$ = 1·25 DEGREES PER SWEEP

An attempt to resolve the problem was made by further simplification of the target. An elementary periodic target was constructed, consisting of two parallel rods of 0.63 cm diameter, spaced on 2.54 cm centres. As the rod spacing was much smaller than that of the multiple rod target, the diffraction pattern (for a double slit) had maxima which had sufficient angular separation to be individually resolved and recorded by the receiving system. This may not have been possible in the case of the multiple-rod target, for which adjacent maxima may not have been resolved.

The observed double slit reverberation pattern is shown in Figure 4.3.4 for angles of incidence on one side of the axis, and the calculated positions of the maxima in Figure 4.3.5, for the same ranges of angle and frequency. The agreement between the two figures was excellent at angles of incidence $\theta \geqslant 25^{\circ}$, but in the range $0^{\circ} < \theta < 15^{\circ}$ the expected pattern becomes indistinct, and appears to be obscured by a different pattern, while in the intermediate region $15^{\circ} < \theta < 25^{\circ}$ it was difficult to say which pattern was dominant. Attempts to explain these unexpected features in terms of diffraction phenomena were unsuccessful, but it was observed that the lines of maximum intensity in the low angle region of the pattern had slopes opposite to those of the calculated pattern and greater in magnitude. Any explanation of the observed pattern had to account successfully for this change in character.

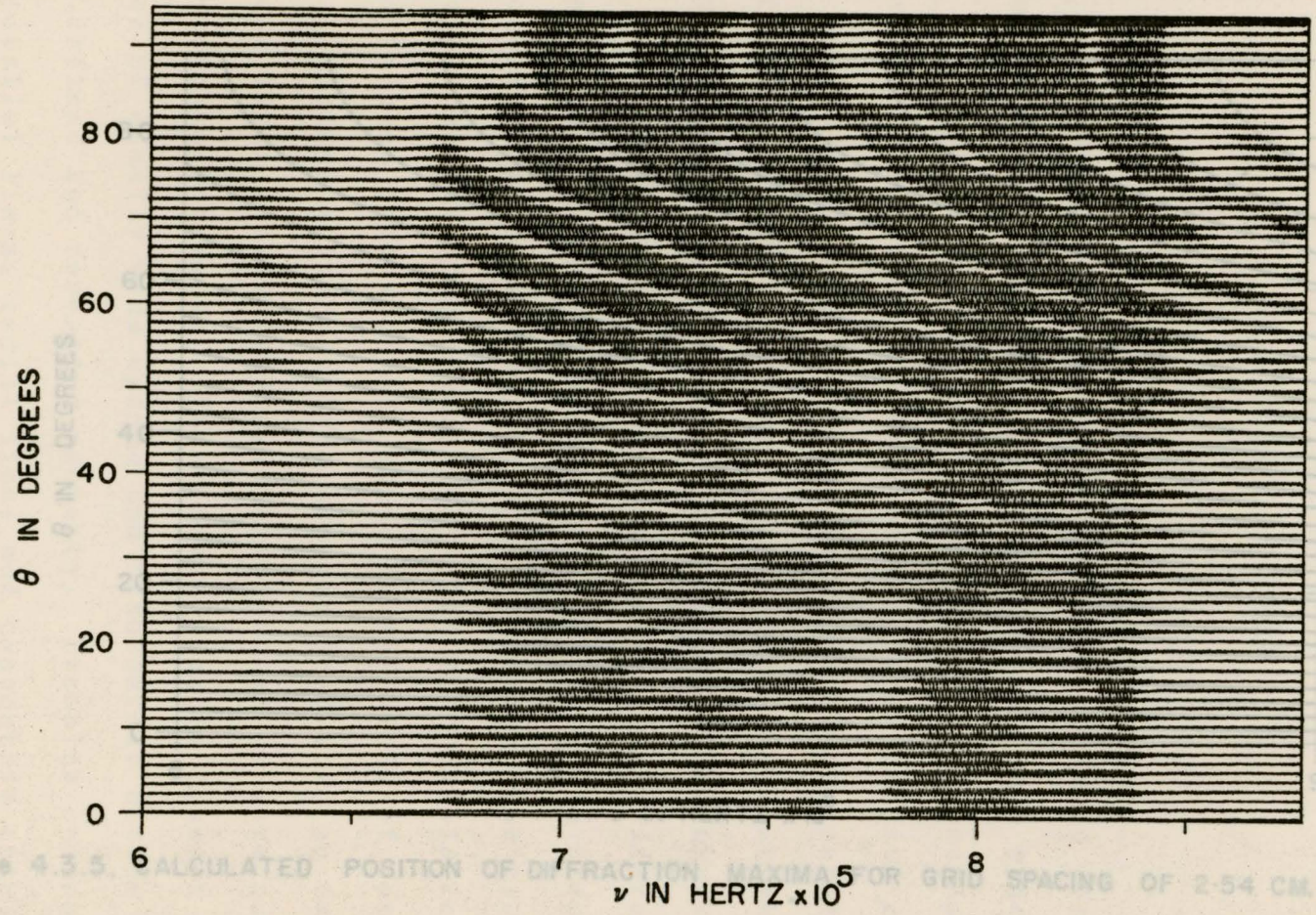

Figure 4.3.4. REVERBERATION FROM TWO RODS, SPACING 2·54 CM.

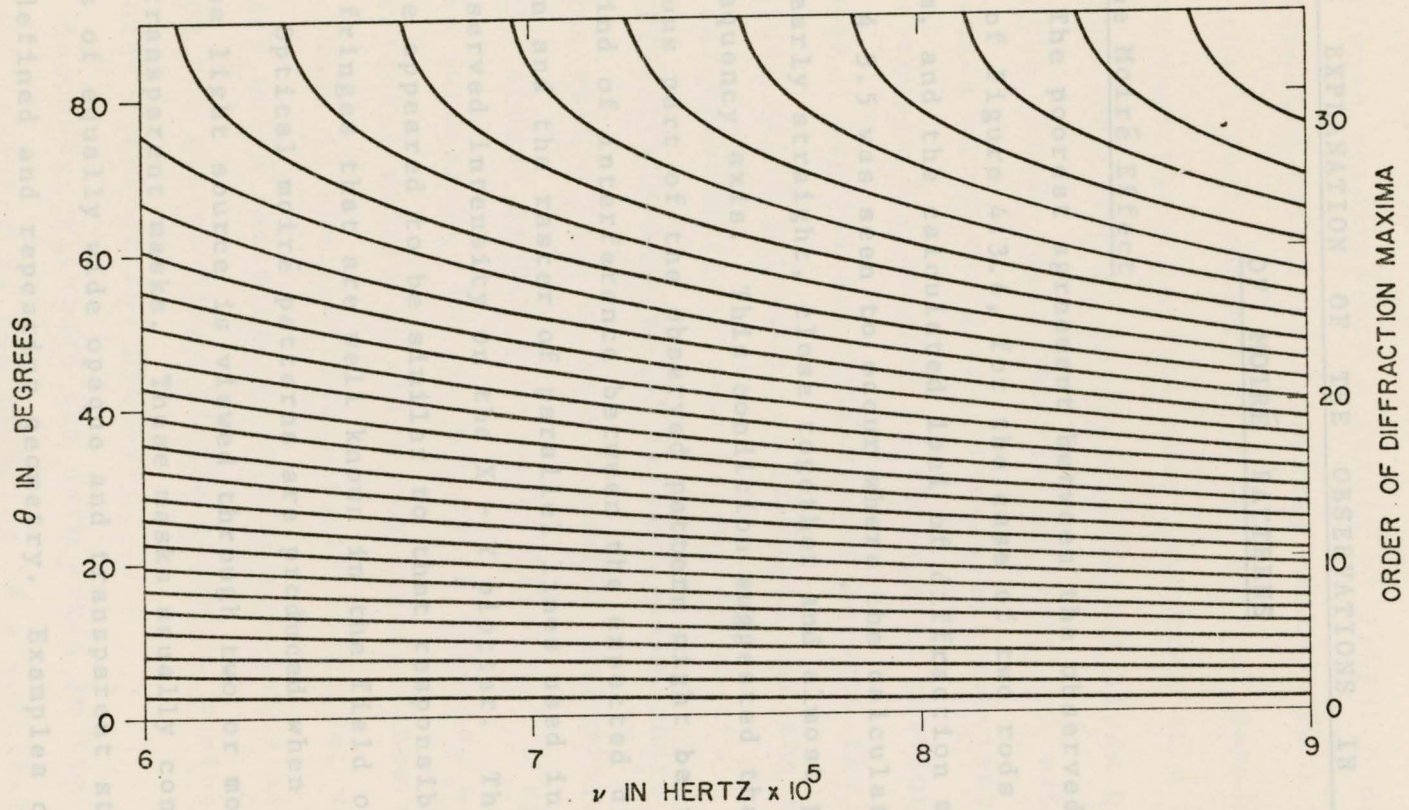

Figure 4.3.5. CALCULATED POSITION OF DIFFRACTION MAXIMA FOR GRID SPACING OF 2·54 CM.

CHAPTER 5

AN EXPLANATION OF THE OBSERVATIONS IN TERMS OF MOIRÉ PATTERNS

5.1 The Moiré Effect

The poorest agreement between the observed intensity curves of Figure 4.3.4, for the case of two rods spaced at 2.54 cm, and the calculated loci of diffraction maxima in Figure 4.3.5 was seen to occur where the calculated curves were nearly straight, close together and almost parallel to the frequency axis. This condition suggested that the anomalous part of the observed pattern might be the result of some kind of interference between the expected diffraction pattern and the raster of parallel lines used in displaying the observed intensity on the X - Y plotter. The type of interference appeared to be similar to that responsible for the moiré fringes that are well known in the field of optics.

Optical moiré patterns are produced when an extended diffuse light source is viewed through two or more superposed semi-transparent masks. These masks usually consist of a series of equally wide opaque and transparent strips having a well defined and repeating geometry. Examples commonly met are parallel lines, radial lines and concentric circles; these and other geometries were discussed by Oster and Nishijima (1963) and others. Such masks may be considered as amplitude

gratings with a 50% transmission ratio. The light and dark moiré fringes observed are a result of slight angular displacement or spacing differences between masks. In a typical moiré pattern the effect appears when two sets of parallel straight lines are superposed so that they intersect at a small angle. The fringes then appear as broad parallel lines bands bisecting the obtuse angle between the original sets of lines. Dark fringes occur where the transparent portions of one mask are most completely covered by the opaque portions of the other mask. Significant differences between the masks by which the optical moiré patterns are produced and the equivalent arrays in the acoustical case become apparent.

First, the dark moiré fringes occur where a raster line coincides with a line of high acoustic intensity, rather than where the opaque raster line would "fill in" a space of low acoustic intensity. In optical moiré effects, a <u>light</u> fringe joins adjacent points at which the centre-lines of the <u>translucent</u> bands in the individual masks coincide; whereas, in the acoustics moiré patterns, a <u>dark</u> fringe joins adjacent points at which the centre-lines of the acoustic maxima coincide with the raster lines of the plotter.

Secondly, although the dark areas in the acoustic patterns are produced by the addition of a vertical oscillation or"wobble" of variable width to the nearly horizontal sweep of the raster lines, the acoustic intensity is measured with an angular resolution that is much sharper than might be in-

ferred from the wobble amplitude that portrays it. The raster, considered as a mask, would have its opaque and transparent "lines" of very unequal widths.

Thirdly, the intensity of the acoustic diffraction pattern does not correspond to sharply defined opaque and transparent bands of equal width. For reflection from a pair of simple rods, the intensity varies sinusoidally with angle at a given frequency; however, for reflection from a regular grid of n parallel rods, the intensity will exhibit strong principal maxima separated by n-1 minima, and n-2 weak secondary maxima, as for an optical diffraction grating.

In spite of these differences, the optical moiré fringes produced by superposing the wobble-free raster lines of Figure 5.1.1 and the calculated acoustic diffraction pattern of Figure 4.3.5, as in Figure 5.1.2, produced in a general way the main features of the observed pattern of Figure 4.3.4.

5.2 The Graphical Construction

Figure 5.2.1 reproduces Figures 4.3.4, 4.3.5, 5.1.1 and 5.1.2 on a single page, reduced to a common scale, for greater convenience in comparing features of the "constructed" optical pattern with the observed acoustic pattern. No moiré effect is obvious in the former where the calculated diffraction lines are well spaced and inclined to the raster lines at angles greater than about 15 degrees. The effect is most visible where the angle of inclination lies between 2 and 8 degrees.

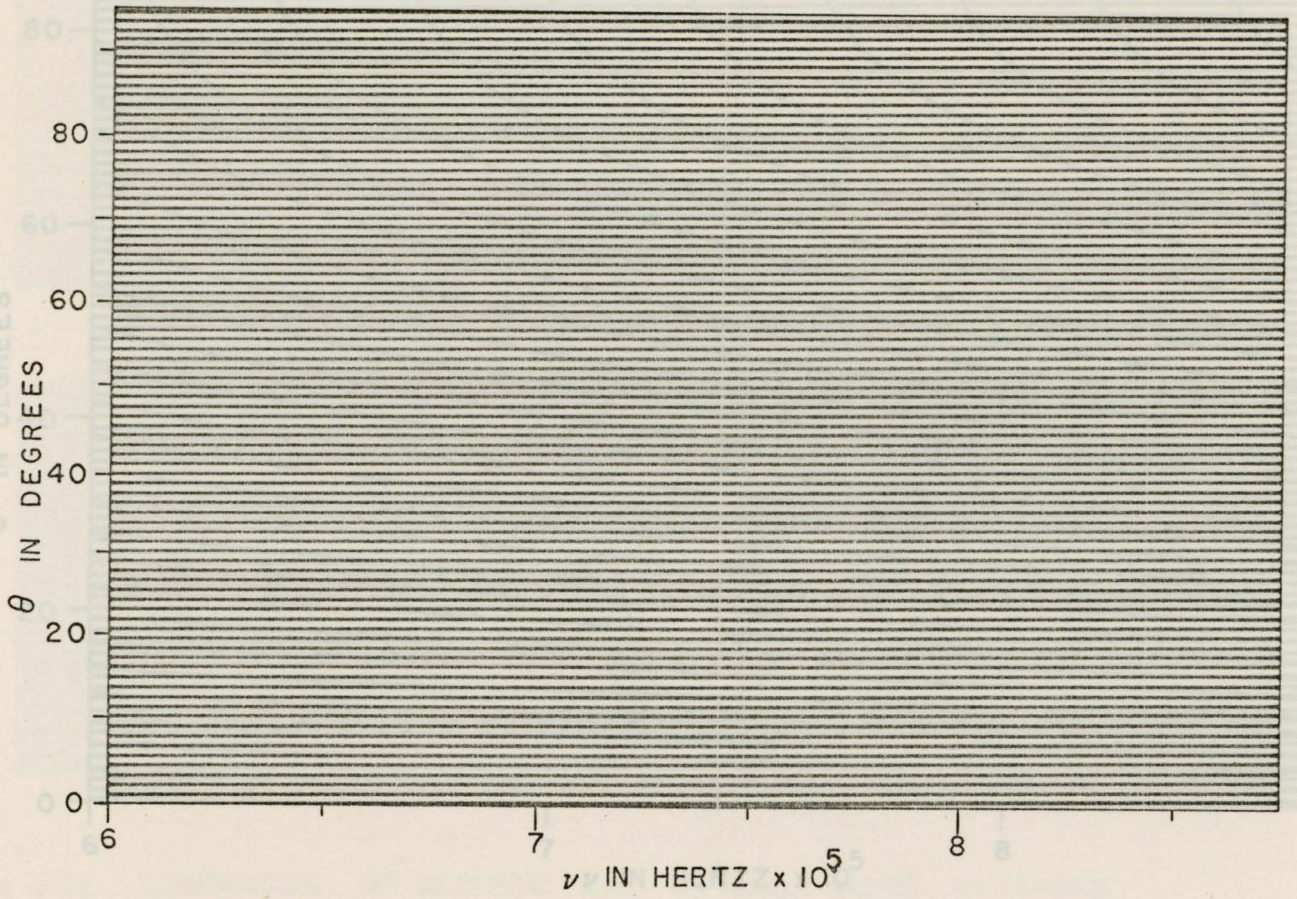

Figure 5.1.1. RASTER SCAN PATTERN FOR ROD SPACING 2·54 CM, TRACED FROM FIGURE 4.3.5.

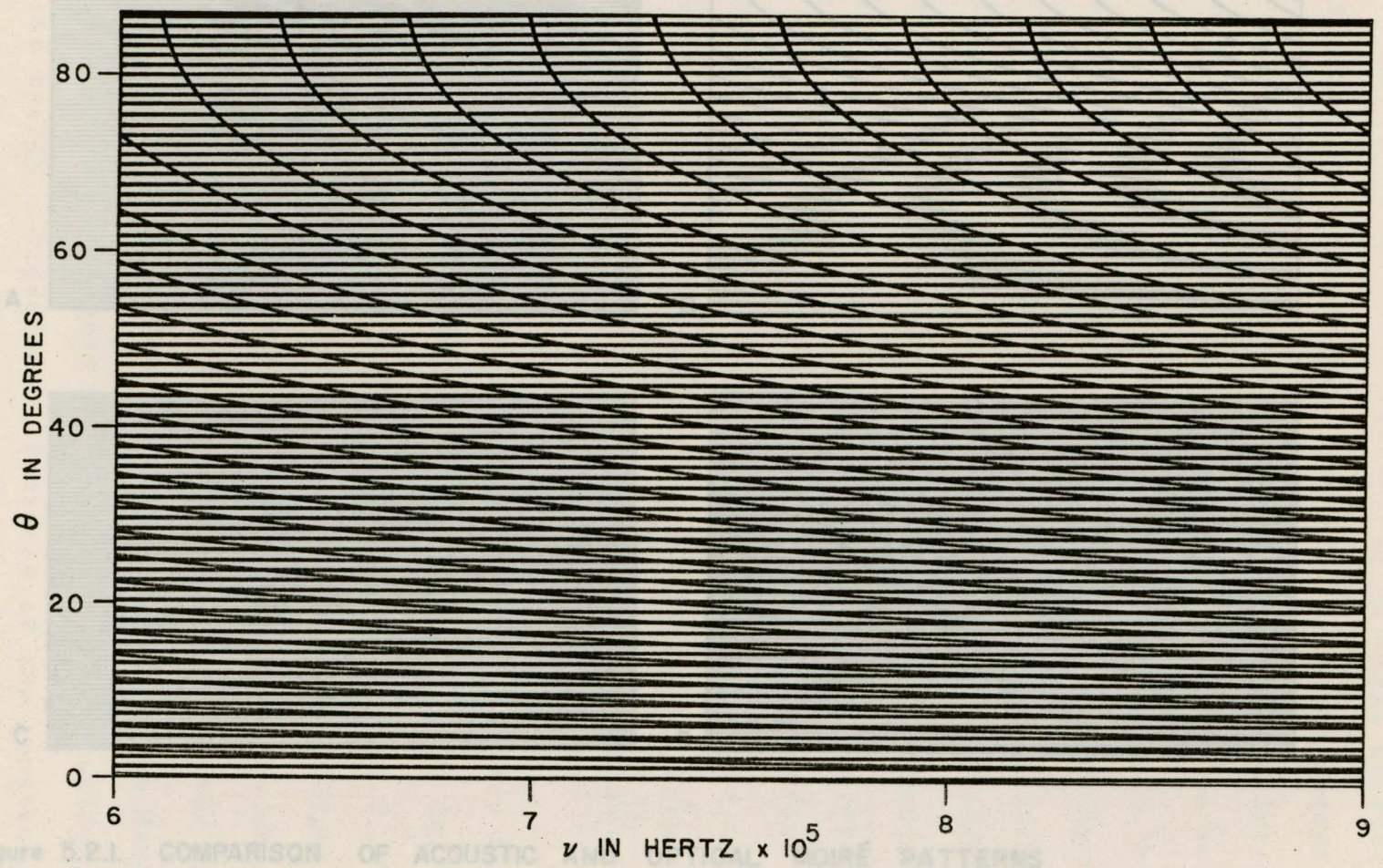

Figure 5.1.2. MOIRÉ CONSTRUCTION FOR ROD SPACING OF 2·54 CM., OBTAINED BY SUPERPOSITION OF FIGURE 4.3.5. WITH FIGURE 5.1.1.

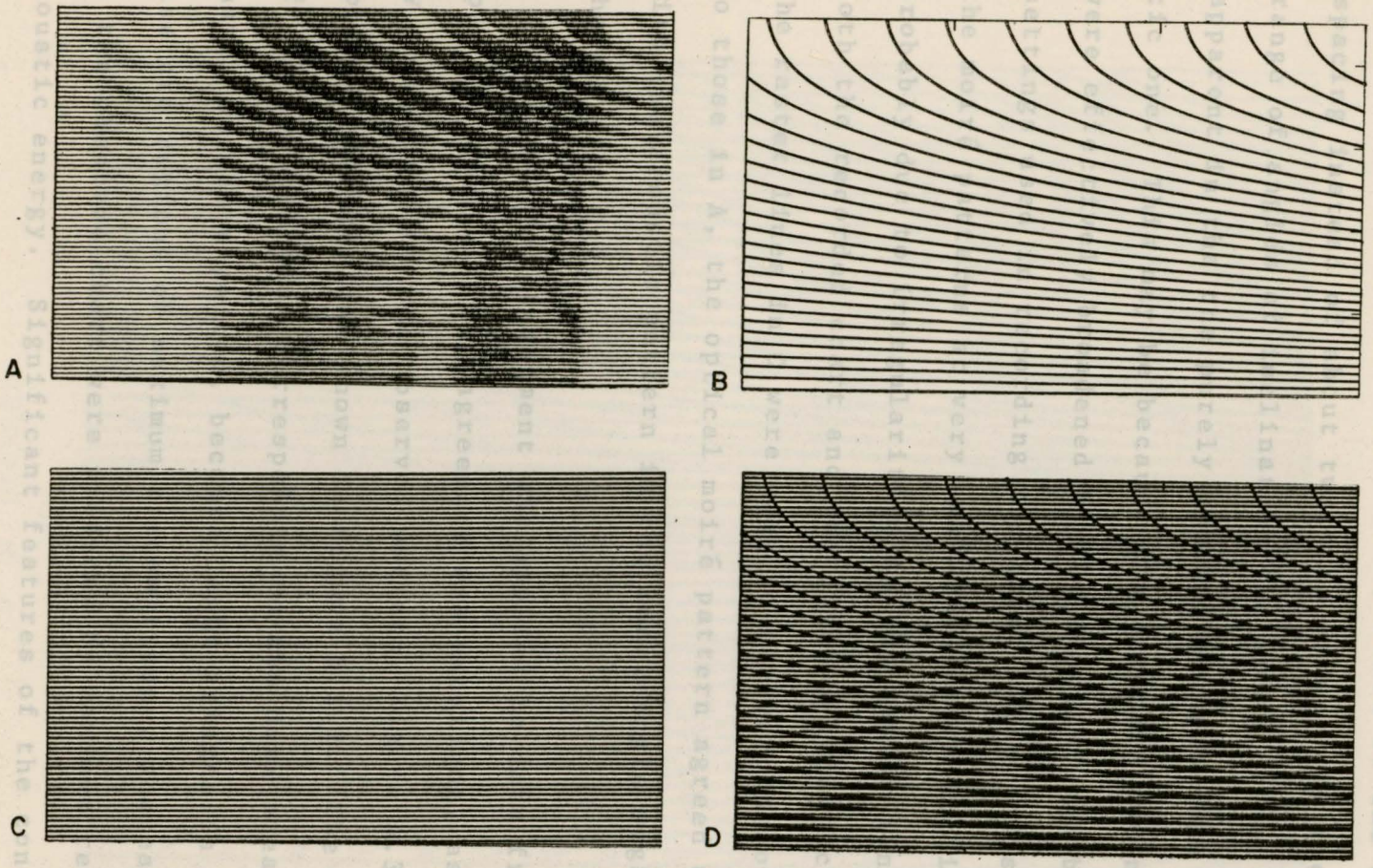

Figure 5.2.1. COMPARISON OF ACOUSTIC AND OPTICAL MOIRÉ PATTERNS

A. ACOUSTIC PATTERN (Figure 4.3.4.); B. CALCULATED DIFFRACTION PATTERN (Figure 4.3.5.)

C. REFERENCE RASTER (Figure 5.1.1.); D. OPTICAL PATTERN FROM B AND C COMBINED.

The fringe contrast would presumably be still greater if the diffraction line spacing was comparable to the raster line spacing instead of about twice as large. In the intermediate range of angles of inclination the moiré effect is more apparent in the the purely optical example than in the acoustic one. This may be because the acoustic intensity maxima were effectively broadened by the contrast and bias control settings used in recording the chart. The indistinctness of the moiré patterns at very small angles of inclination is probably due to irregularities in the raster line spacing for both the recorded chart and the optical construction. When the raster lines in C were made to correspond more closely to those in A, the optical moiré pattern agreed more closely with the acoustic pattern in the small-angle region of the chart.

A similar treatment was applied to data from the multiple rod target. The agreement was excellent, as can be seen by comparison of the observed pattern, Figure 4.3.2, with the optical construction shown in Figure 5.2.2. The light fringes of the construction corresponded to the dark areas on the chart, as was expected, because light fringes in the optical case are regions of maximum transmittance, whereas dark areas on the observed chart were produced by maximum reflection of acoustic energy. Significant features of the construction were that it reproduced the shape of the star pattern and

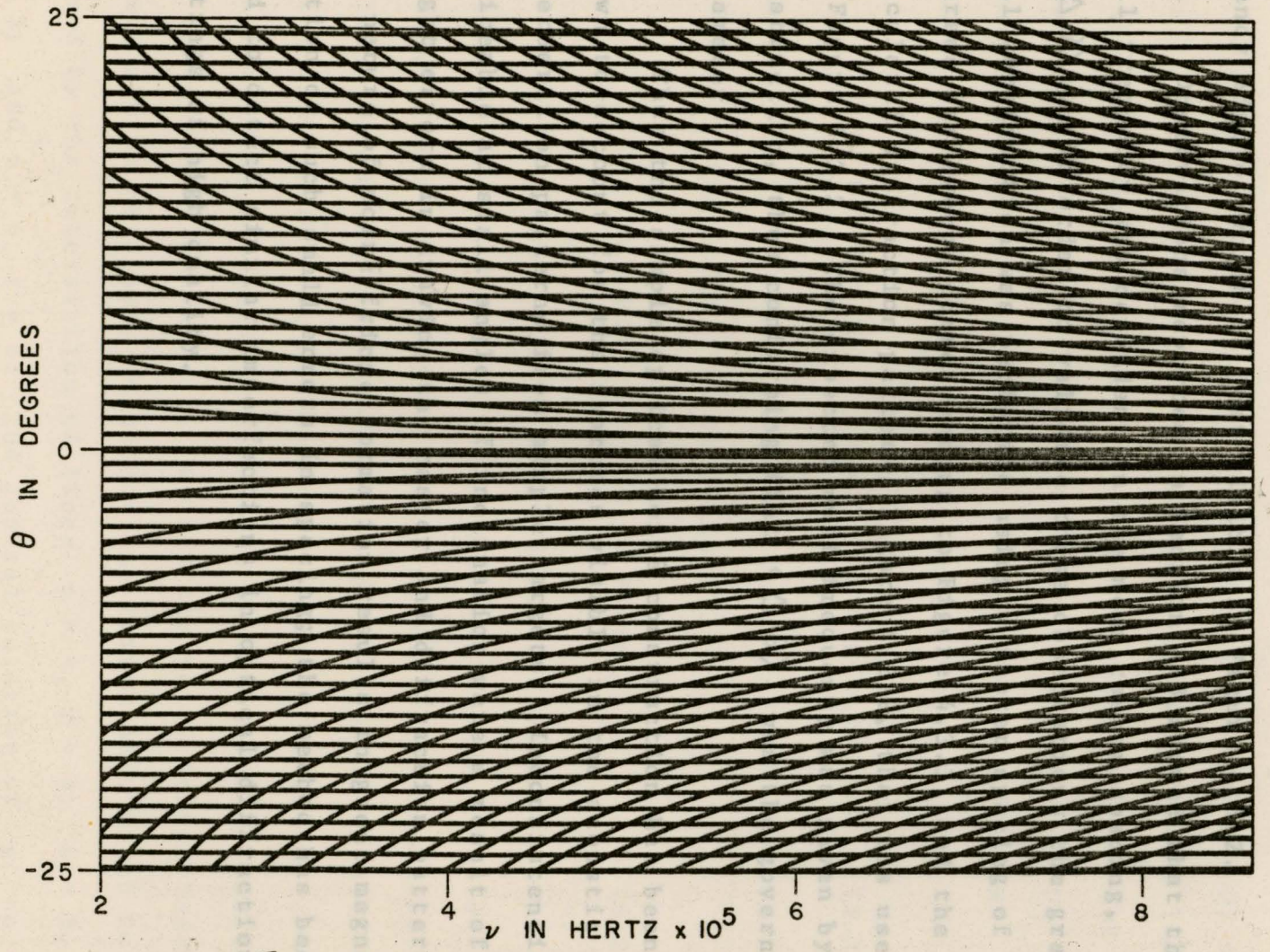

Figure 5.2.2. MOIRÉ FRINGE CONSTRUCTION FOR ROD SPACING 6·72 CM, $\langle \Delta\theta \rangle$ = 1·25 DEGREES PER SWEEP

predicted accurately the frequency of the null point at 685 kHz. It also showed another star pattern, somewhat less distinct, with a null frequency of about 320 kHz, the high frequency edge of which is just visible in Figure 4.3.2.

Observations reported in Section 4.3 showed that the null frequency was dependant on the mean raster spacing, $\langle \Delta \theta \rangle$. In order to validate these observations the graphical construction was performed using a raster spacing of 1.25 degrees per sweep, corresponding to Figure 4.3.3, and the same calculated diffraction pattern, Figure 4.2.2, that was used in Figure 5.2.2. The expected null frequency was given by the construction, thus confirming that $\langle \Delta \theta \rangle$ was the governing parameter.

Thus the simple optical moiré construction has been shown to account for the features visible in the acoustic reverberation patterns from simple targets. Inconsistencies noticeable at small angles of inclination were a result of slight errors in drawing the raster and diffraction patterns. The nature of moiré fringe formation results in great magnification of such small errors in spacing; the method has been used to detect similar imperfections in optical diffraction gratings of high quality.

5.3 An Analytical Interpretation

The relation between moiré fringes and the superimposed families of lines which give rise to them in the optical case has been studied by Oster et al (1964), Theocaris (1969) and Durelli and Parks (1970). In general, two families of lines in the x,y plane can be represented by equations of the form $f(x,y,r) = 0$, and $f(x,y,n) = 0$, where r and n are parameters which index the lines in the respective families. If each equation is solved for its index, so that

$$r = r(x,y) \quad \text{and} \quad n = n(x,y) \tag{5.1}$$

then the family of resulting moiré fringes can be expressed in terms of its index, m, as follows

$$m = m(x,y) = r(x,y) + n(x,y) \tag{5.2}$$

The treatment can be adapted for the acoustic case with reference to Figure 5.3.1, which represents a raster of parallel lines overlaid by a family of diffraction curves (solid), and shows the resulting moiré fringes (broken). The raster line index, r, and the diffraction line index, n, have both been arbitrarily chosen to increase for θ increasing. The relationship between r, n, and the moiré fringe index, m, may now be obtained. Consider the fringe ABC, which is formed by the intersection of lines $n = 4$, $r = 4$; $n = 5$, $r = 5$; and $n = 6$, $r = 6$. The general relation of n to r for this fringe $r - n = 0$, and the fringe is designated as

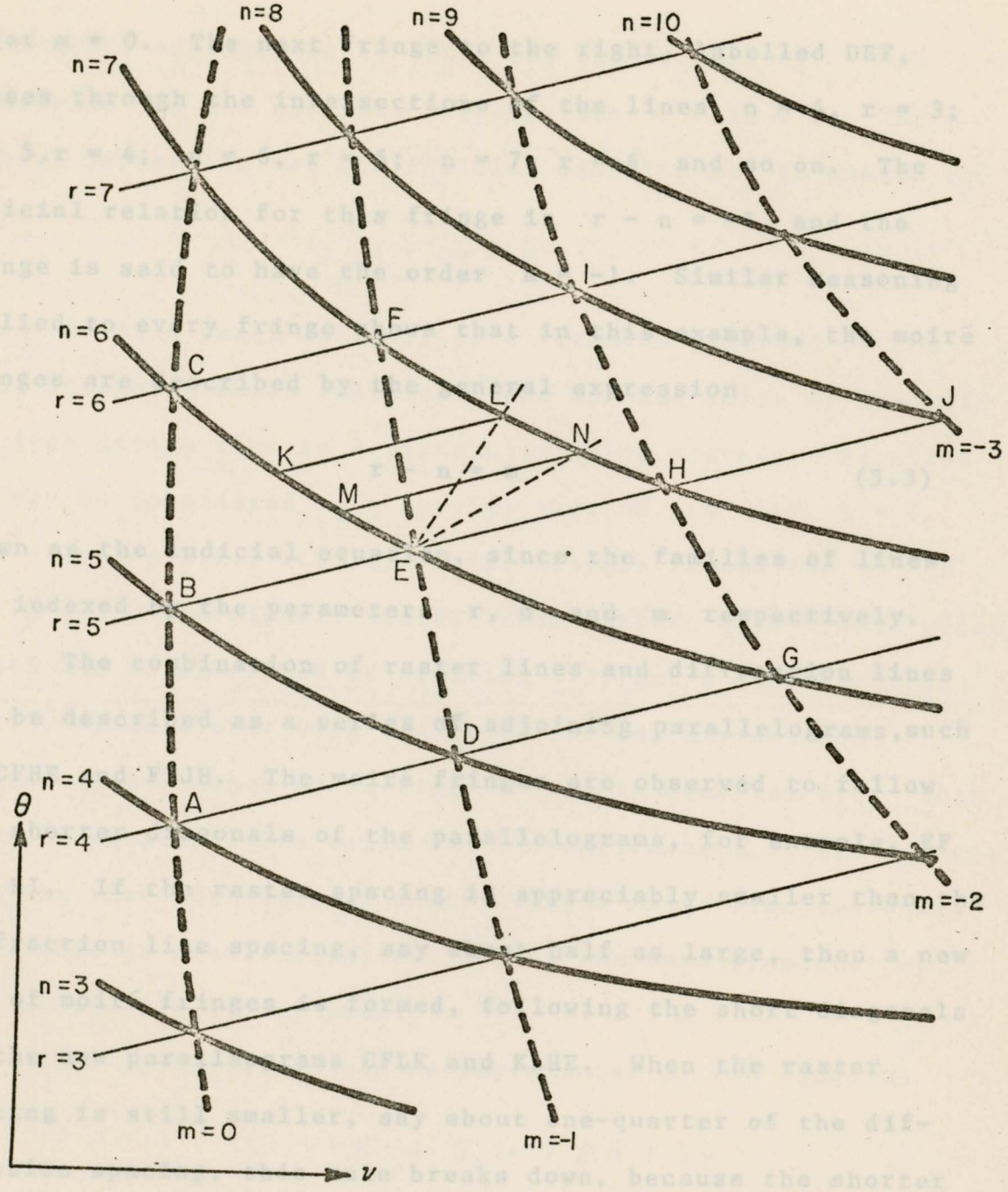

Figure 5.3.I. INDICIAL REPRESENTATION OF MOIRÉ FRINGE FORMATION

order m = 0. The next fringe to the right, labelled DEF, passes through the intersections of the lines n = 4, r = 3; n = 5,r = 4; n = 6, r = 5; n = 7, r = 6 and so on. The indicial relation for this fringe is r - n = -1, and the fringe is said to have the order m = -1. Similar reasoning applied to every fringe shows that in this example, the moiré fringes are described by the general expression

$$r - n = m \qquad (5.3)$$

known as the indicial equation, since the families of lines are indexed by the parameters r, n and m respectively.

The combination of raster lines and diffraction lines may be described as a series of adjoining parallelograms,such as CFHE and FIJH. The moiré fringes are observed to follow the shorter diagonals of the parallelograms, for example, EF and HI. If the raster spacing is appreciably smaller than the diffraction line spacing, say about half as large, then a new set of moiré fringes is formed, following the short diagonals of the new paralleograms CFLK and KLHE. When the raster spacing is still smaller, say about one-quarter of the diffraction spacing, this rule breaks down, because the shorter diagonals ML and EN of the new parallelograms, KLNM and MNHE are longer than the diagonals of the parallelograms formed by doubling the spacing. The moiré fringes will still follow the shortest diagonal, but in that case will appear in a di-

rection EL, appropriate to twice the raster spacing. This gives rise to the new indicial equation $r - 2n = m$. The general expression for the indicial equation may be stated as

$$r - hn = m \qquad (5.4)$$

where h is a small integer, or a fraction composed of two small integers, which represents the spacing ratio of the sets of lines giving rise to a particular moiré pattern. Equation 5.3 may be considered as a special case of 5.4 with $h = 1$.

Figure 5.2.2 displays moiré fringes formed for $h = 1$ and $h = 2$. The clearly visible star pattern with a null point at 685 kHz is described by equation 5.3, but a somewhat less clearly visible star with a null at 320 kHz may only be adequately explained by setting $h = 2$ in equation 5.4. Both indicial equations are valid for the entire area of the figure, implying that both sets of moiré fringes exist simultaneously. While this is true analytically, only the more prominent set will be visible at any point.

The raster lines can be represented by the equation

$$\theta = \theta_0 + r\,\Delta\theta + R\nu$$

where $\Delta\theta$ is the uniform separation of the raster lines, R is their slope and θ_0 is the θ intercept for the line designated $r = 0$. Solving for the index gives

$$r = (\theta - \theta_0 - R\nu)/\Delta\theta . \qquad (5.5)$$

The curves of maximum acoustic intensity, for reflection from a pair of parallel rods with a separation d, are given by

$$2d \sin\theta = nc/\nu$$

where the order of interference, n, serves as the index. Solving for n gives

$$n = \nu\,(2d/c)\sin\theta \qquad (5.6)$$

Then the index for the dark fringes of the acoustic moiré pattern is given by the indicial equation 5.3

$$m = r - n = (\theta - \theta_0 - R\nu)/\Delta\theta - \nu(2d/c)\sin\theta \qquad (5.7)$$

Because of the way in which θ appears twice in this equation, ν is the more convenient dependent variable. For the m^{th} fringe the expression relating ν and θ with the constants of the acoustic diffraction pattern, c and d, the constants of the raster pattern, θ_0, $\Delta\theta$ and R, becomes

$$\nu_m = \frac{m\,\Delta\theta - \theta + \theta_0}{-R - (2d\,\Delta\theta/c)\sin\theta} \qquad (5.8)$$

A short program was written in BASIC to solve Equation 5.8 numerically on the Physics Department PDP-11/10 computer (see Appendix B). The moiré patterns were calculated for the data of Figures 4.3.2 and 4.3.3, and are shown in Figures 5.3.2 and 5.3.3 respectively. The calculated positions of the moiré fringes are in good agreement with the experimental data,

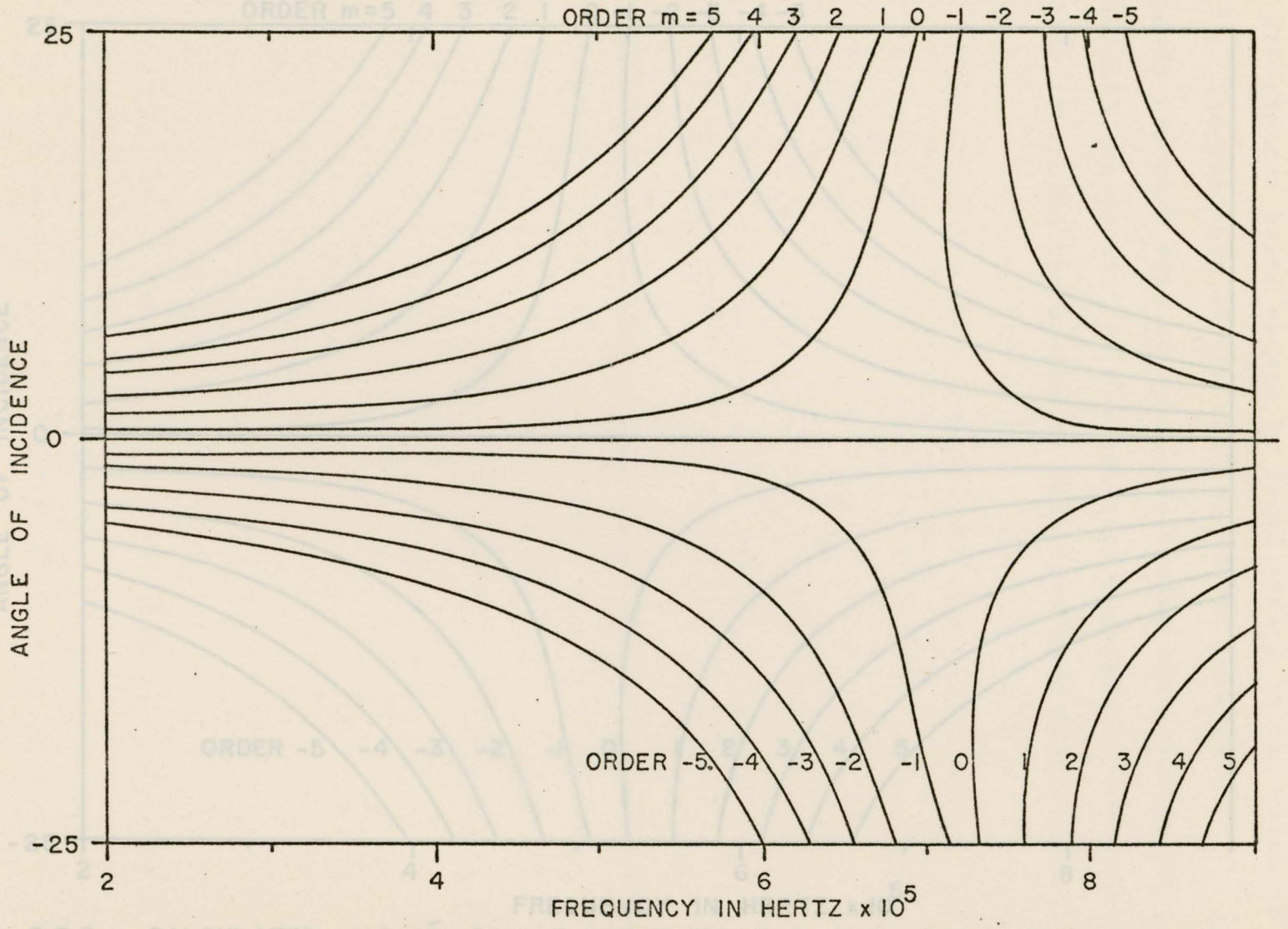

Figure 5.3.2. CALCULATED MOIRÉ FRINGE POSITIONS FOR DATA FROM FIGURE 4.3.2.

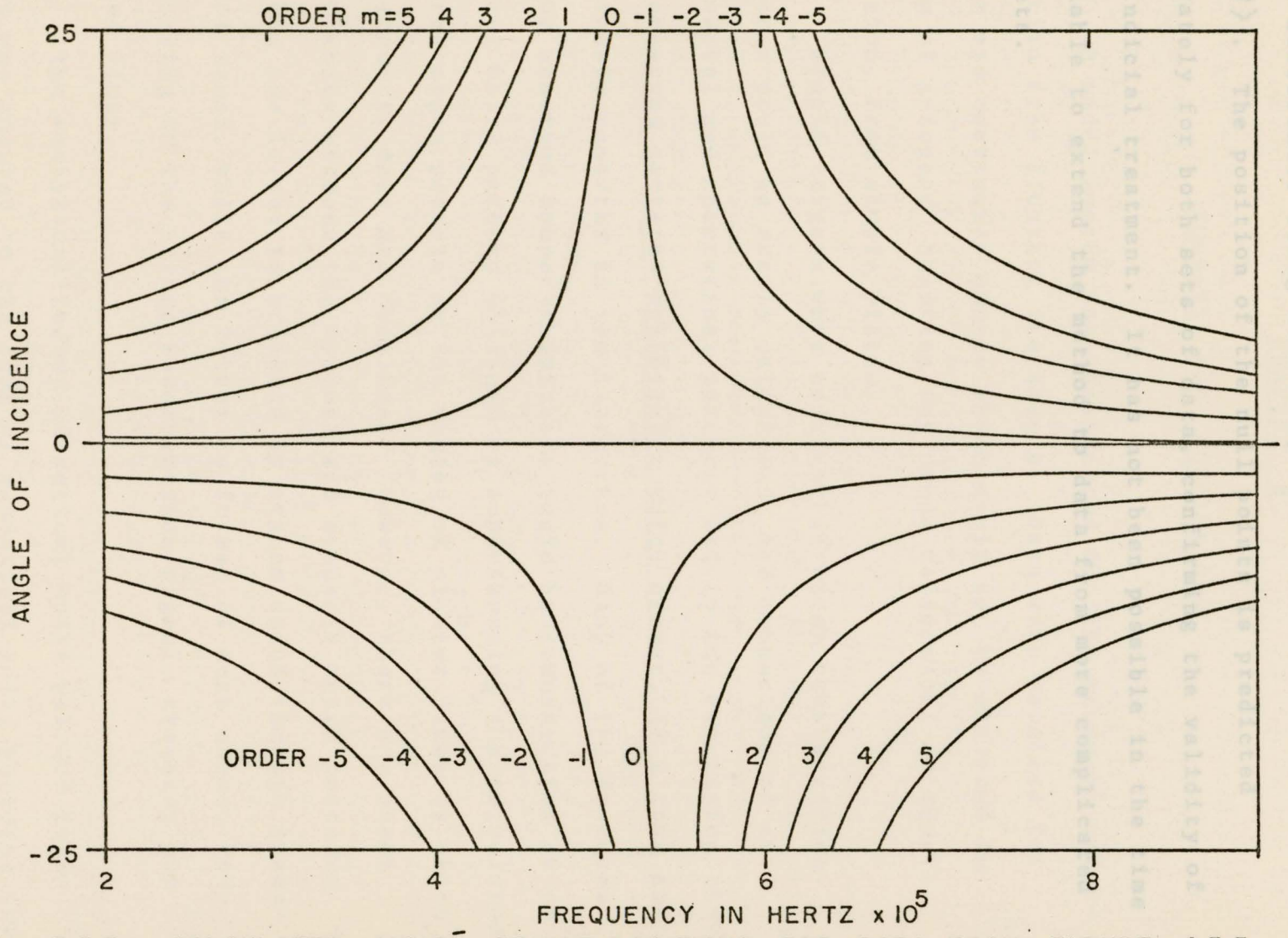

Figure 5.3.3. CALCULATED MOIRÉ FRINGE POSITIONS FOR DATA FROM FIGURE 4.3.3.

small differences being caused by local errors in the value of $\langle \Delta \theta \rangle$. The position of the null points is predicted accurately for both sets of data, confirming the validity of the indicial treatment. It has not been possible in the time available to extend the method to data from more complicated targets.

CHAPTER 6

SUMMARY AND CONCLUSIONS

A model system was constructed for the study of reverberation from floating ice sheets. Data were obtained for plane and corrugated sheets which could not be analysed in terms of accepted theories for sound reflection, or reverberation, from simple plates.

Simple targets were constructed whose reverberation patterns could be easily calculated, and comparison of experimental and theoretical patterns led to the conclusion that the observed patterns exhibited a moiré effect, of a type not previously reported in the literature. Many of the features of the observed acoustic patterns could be demonstrated as an optical moiré pattern obtained by superimposing the calculated reverberation pattern on the raster of plotter lines by which the acoustic data are displayed. However, there are phase differences between the optical and acoustic moiré patterns because the former is produced by transmission through transparent areas, while the latter is formed of dark areas, corresponding to the strong reverberation signal, crossing the raster lines.

The analytical theory of optical moiré pattern formation was adapted to the case of acoustical moire patterns for the relatively simple reverberation from a pair of parallel

rods. Although the theory is such that the true acoustic reverberation pattern fron any target should be recoverable from the moire patterns formed by the type of display used, the lack of an analytical expression for the moiré pattern would require the use of numerical methods which have not been attempted.

The development of such numerical methods would be appropriate as an extension of the work reported in this thesis. Equipment is already available in this laboratory to enable reverberation data to be digitised on-line and recorded on computer-compatible magnetic tape in real time, ready for subsequent analysis. A custom-built data logger can record the following six pieces of data for each transmitted tone-burst; the duration of the tone-burst in microseconds, the number of cycles of sine-wave from the function generator, a voltage proportional to the signal strength, a voltage proportional to the angle of incidence, a voltage proportional to the step attenuator setting, and one uncommitted analogue voltage. This information, together with frequency response calibration curves for the transducers used, should be sufficient to provide a computer with the data from which a point to point intensity map of the underlying acoustic reverberation pattern could be calculated. An advantage of computer processing would be the ability to correct the data for non-uniform frequency response of the transducers.

A different approach, involving less instrumentation might be to use the existing $\nu - \theta$ charts and digitize the centre-lines of the visible moire fringes by means of a two-dimensional digitization. Data in this form would be easier to handle than the raw data mentioned above, but would contain only qualitative information on the true reverberation pattern.

REFERENCES

Baborovsky, W. M. and Marsh, D. M. 1971. A Schlieren Study of Ultrasonic Pulse Propagation and Reflection. Proceedings of the Ultrasonics Conference, London, September 28-29, 1971. I. P. C. Science and Technology Press, Ltd., Guildford, Surrey, England.

Barss, W. M. July, 1972. Canadian Patent Number 904968.

Chapman, R. P. and Scott, H. D. 1966. Backscattering Strengths of Sea Ice. J. Acoust. Soc. Am., 39, 1191-1193.

Dragonette, L. R. 1972. Schlieren Visualisation of Radiation Caused by Illumination of Plates with Short Acoustic Pulses. J. Acoust. Soc. Am., 51, 920-935.

Durelli, A. J. and Parks, V. J. 1970. Moiré Analysis of Strain. Prentice-Hall, Inc., Englewood Cliffs, N. J. U. S. A.

Fay, R. D. 1946. Non-specular Reflection of Sound from Submerged Plates. Massachusetts Institute of Technology Acoustics Laboratory Technical Memorandum No. 7.

_____. 1948. Interactions Between a Plate and a Sound Field. J. Acoust. Soc. Am., 20, 620-625.

_____, and Fortier, O. V. 1951. Transmission of Sound through Steel Plates Immersed in Water. J. Acoust. Soc. Am., 23, 339-346.

Finney, W. J. 1948. Reflection of Sound from Submerged Plates. J. Acoust. Soc. Am., 20, 626-637.

Horton, J. W. 1965. Fundamentals of Sonar. U. S. Naval Institute, Annapolis, U. S. A.

Hunkins, K. 1960. Seismic Studies of Sea Ice. J. Geophys. Research, 65, 3459-3472.

Kinsler, L. E. and Frey, A. R. 1962. Fundamentals of Acoustics. John Wiley and Sons, Inc., New York, U. S.A.

Kutschale, H. 1969. Arctic Hydroacoustics. Arctic, 22, 246-264.

Lamb, H. 1917. On Waves in an Elastic Plate. Proc. Roy. Soc. (London), Series A, 93, 114.

Langleben, M. P. 1970. Reflection of Sound at the Water-Sea Ice Interface. J. Geophys. Research, 75, 5243-5246.

Lyon, W. 1961. Ocean and Sea Ice Research in the Arctic Ocean via Submarine. Transactions of the N. Y. Academy of Sciences II, 23, 662-674.

Marsh, H. W. and Mellen, R. H. 1963. Underwater Sound Propagation in the Ocean. J. Acoust. Soc. Am., 35, 552-563.

McKee, A. C. 1973. Acoustic Interchange Between a Liquid and a Floating Solid Plate. M.Sc. Thesis, University of Victoria, Victoria, British Columbia.

Mellen, R. H. and Marsh, H. W. 1963. Underwater Sound Reverberation in the Arctic Ocean. J. Acoust. Soc. Am., 35, 1645-1648.

Milne, A. R. 1967. Sound Propagation and Ambient Noise Under Sea Ice. Underwater Acoustics, 2, 103-138.

Osbourne, M. F. M. and Hart, S. D. 1945. Transmission, Reflection and Guiding of an Exponential Pulse by a Steel Plate in Water. J. Acoust. Soc. Am., 17, 1-18.

Oster, G. and Nishijima, Y. May 1963. Moiré Patterns. Scientific American, 208, 54-69.

_____, Wasserman, M. and Zwerling, C. 1964. Theoretical Interpretation of Moiré Patterns. J. Opt. Soc. Am., 54, 169-174.

Pierce, G. W. 1936. U. S. Patent Number 2,063,944.

Pounder, E. R. 1955. The Physics of Ice. Pergamon Press, Ltd., Oxford, England.

Press, F. and Ewing, M. 1951. Propagation of Elastic Waves in a Floating Ice Sheet. Trans. Am. Geophys. Union, 32, 673-678.

Rayleigh, Lord (J. W. Strutt). 1885. On Waves Propagated Along the Plane Surfaces of an Elastic Solid. Proc. London Math.Soc., 17, 4-11.

Lamb, H. 1917. On Waves in an Elastic Plate. Proc. Roy. Soc. (London), Series A, 93, 114.

Langleben, M. P. 1970. Reflection of Sound at the Water-Sea Ice Interface. J. Geophys. Research, 75, 5243-5246.

Lyon, W. 1961. Ocean and Sea Ice Research in the Arctic Ocean via Submarine. Transactions of the N. Y. Academy of Sciences II, 23, 662-674.

Marsh, H. W. and Mellen, R. H. 1963. Underwater Sound Propagation in the Ocean. J. Acoust. Soc. Am., 35, 552-563.

McKee, A. C. 1973. Acoustic Interchange Between a Liquid and a Floating Solid Plate. M.Sc. Thesis, University of Victoria, Victoria, British Columbia.

Mellen, R. H. and Marsh, H. W. 1963. Underwater Sound Reverberation in the Arctic Ocean. J. Acoust. Soc. Am., 35, 1645-1648.

Milne, A. R. 1967. Sound Propagation and Ambient Noise Under Sea Ice. Underwater Acoustics, 2, 103-138.

Osbourne, M. F. M. and Hart, S. D. 1945. Transmission, Reflection and Guiding of an Exponential Pulse by a Steel Plate in Water. J. Acoust. Soc. Am., 17, 1-18.

Oster, G. and Nishijima, Y. May 1963. Moiré Patterns. Scientific American, 208, 54-69.

_____, Wasserman, M. and Zwerling, C. 1964. Theoretical Interpretation of Moiré Patterns. J. Opt. Soc. Am., 54, 169-174.

Pierce, G. W. 1936. U. S. Patent Number 2,063,944.

Pounder, E. R. 1955. The Physics of Ice. Pergamon Press, Ltd., Oxford, England.

Press, F. and Ewing, M. 1951. Propagation of Elastic Waves in a Floating Ice Sheet. Trans. Am. Geophys. Union, 32, 673-678.

Rayleigh, Lord (J. W. Strutt). 1885. On Waves Propagated Along the Plane Surfaces of an Elastic Solid. Proc. London Math.Soc., 17, 4-11.

Sanders, F. H. 1939. Transmission of Sound through Thin Plates. Can. J. Research, 17, 179-193.

Sasaki, S. 1963. Back Reflection of Ultrasonic Wave Obliquely Incident to Solid Surface in Water. Japan. J. Applied Phys., 2, 198.

Smythe, J. B. and Lindsay, R. B. 1944. Supersonic Transmission at Oblique Incidence through a Solid Plate in Water. J. Acoust. Soc. Am., 16, 20-25.

Theocaris, P. S. 1969. Moiré Fringes in Strain Analysis. Pergamon Press, Ltd., Oxford, England.

Viktorov, I. A. 1967. Rayleigh and Lamb Waves : Physical Theory and Applications. Plenum Press, New York, U.S.A.

APPENDIX A

MANUFACTURERS AND MODEL NUMBERS OF ELECTRONIC EQUIPMENT REFERRED TO IN CHAPTER 3

Master pulse generator	Tektronix Type 162 Waveform Generator, Tektronix Inc., Beaverton, Oregon, U. S. A.
Echo pulse generator	Tektronix Type 161 generator - modified to enable the output pulse voltage to be accurately controlled in range 0 to 5 volts.
Frequency offset control	Tektronix Type 161 pulse generator - modified to enable the output pulse voltage to be accurately controlled in the range 0 to 5 volts.
Sweeping function generator	DataRoyal Model F230A Waveform/Sweep Generator, DataRoyal Corporation Inc., San Diego, California, U. S. A. This instrument is now manufactred by Ailtech, 19535 East Walnut Drive, City of Industry, California, U. S. A. (formerly Microdot Inc./Instrumentation Division) - modified to permit the internal ramp generator to be triggered by the gate pulse received next after a frequency sweep. A further modification initiates front panel indication when frequency ranges outside calibration limits.
Power amplifier	Krohn-Hite Model DCA-10R 10 watt Power Amplifier. Krohn-Hite Inc., Cambridge, Mass., U. S. A.
Matching Transformer	Krohn-Hite Model MT-56 50 watt Matching Transformer.

Frequency Counter	T. S. I. Model 361-R Universal Counter. Transistor Specialties Inc., Plainview, Long Island, New York, U. S. A.
Oscilloscope	Solartron CD/1400 Mainframe with CX 1444 Sweep Delay Time Base plug-in, CX 1441 Wide Band Y Amplifier plug-in, CX 1449 Wide Band Differential Y Amplifier plug-in. Solartron Electronics Group Ltd., Farnborough, Hants., England.
Plate positioner	Scientific-Atlanta Model 5103-1 Medium Duty Azimuth Positioner. Scientific Atlanta, Inc., Atlanta, Georgia, U. S. A.
Motor control and angle indicator	Scientific-Atlanta Model 4111 Positioner Control Unit with Indicator Unit.
Pre-amplifiers (2)	Scott Model 141 Low Noise Pre-Amplifier. H. H. Scott Inc., Instrument Division, Maynard, Mass., U.S.A.
X - Y chart plotter	Varian Model F80-A X - Y recorder. Varian, 611 Hansen Way, Palo Alto, California, U. S. A.
D. C. power supply	Hewlett-Packard Model 6215A Bench Series D. C. Power Supply. Harrison Division of Hewlett Packard Co., 100 Locust Ave., Berkeley Heights, New Jersey, U. S. A.
A. C. voltmeter	Hewlett-Packard Model 400F1 A. C. Voltmeter. Hewlett Packard Co., P. O. Box 301, Loveland, California, U. S. A.

APPENDIX B

COMPUTER PROGRAM TO CALCULATE MOIRÉ FRINGE PATTERN

This is a listing of the program named MOIR Ø5, written in BASIC-PLUS.

```
MOIRØ5
10 REM-PROGRAM TO CALCULATE MOIRE FRINGE PATTERN FROM
20 REM-INDICIAL EQUATION R-N=M FOR DOUBLE ROD TARGET
50 INPUT "VELOCITY OF SOUND IN M/SEC";C
60 INPUT "ROD SPACING IN M";D
70 INPUT "RASTER SPACING IN DEGREES";Y
80 INPUT "LENGTH OF CHART IN KHZ";X
90 INPUT "THETA INTERCEPT IN DEGREES";TØ
100 INPUT "RANGE OF THETA";T1;"TO";T2;"IN STEPS OF";T3
110 INPUT "RANGE OF M";M1;"TO";M2
115 FOR M=M1 TO M2 STEP 1
120 PRINT:PRINT"M=";M
130 FOR T=T1 TO T2 STEP T3
140 LET T5=T*3.14159/180
150 LET R=Y/(X*1000)
160 LET B1=M*Y-T+TØ
170 LET B2=-R-(2*D*Y*SIN(T5)/C)
180 LET F=B1/(B2*1000)
190 IF F<100 GOTO 300
200 IF F>2000 GOTO 400
210 PRINT F,
220 NEXT T
230 NEXT M
240 STOP
300 PRINT "UNDER",
310 GOTO 220
400 PRINT "OVER",
410 GOTO 220
500 END
```

A sample of the output is included on the following pages.

```
MOIL05  02:32 PM        27-FEB-74
VELOCITY OF SOUND IN M/SEC? 1480
ROD SPACING IN M? 0.0672
MASTER SPACING IN DEGREES? 1.25
LENGTH OF CHART IN MM? 700
THETA INTERCEPT IN DEGREES? -0.30
RANGE OF THETA? 1  TO  25  IN STEPS OF  1
RANGE OF M? -5  TO  5

M=-5
OVER
 919.34        1487.66        1236          1087.18        988.949
 748.557       867.504        827.47        795.676        769.871
 681.799       730.734        715.575       702.634        691.478
 648.765       673.361        665.974       659.49         653.786
               644.345        640.457       637.045        634.062

M=-4
 1672.51       1270.17        1074.22       958.367        881.92
 827.772       787.476        756.381       731.715        711.723
 695.241       681.465        669.822       659.895        651.369
 644.005       637.62         632.065       627.225        623.006
 619.329       616.133        613.365       610.979        608.94

M=-3
 1340.66       1052.67        912.439       829.554        774.891
 736.205       707.448        685.293       667.754        653.576
 641.925       632.226        624.069       617.155        611.26
 606.212       601.879        598.156       594.96         592.225
 589.894       587.922        586.273       584.914        583.819

M=-2
 1008.81       835.178        750.659       700.741        667.862
 644.637       627.42         614.204       603.793        595.429
 588.609       582.987        578.317       574.416        571.151
 568.418       566.138        564.247       562.696        561.444
 560.458       559.711        559.181       558.848        558.698

M=-1
 676.968       617.684        588.879       571.929        560.833
 553.069       547.392        543.116       539.832        537.281
 535.293       533.749        532.564       531.677        531.042
 530.624       530.397        530.338       530.431        530.663
 531.022       531.5          532.068       532.782        533.577

M= 0
 345.121       400.19         427.099       443.116        453.804
 461.501       467.364        472.027       475.871        479.134
 481.977       484.51         486.811       488.937        490.933
 492.83        494.656        496.429       498.166        499.882
 501.586       503.288        504.996       506.717        508.455
```

```
M= 0
 345.121        400.19          427.099         443.116         453.804
 461.501        467.364         472.027         475.871         479.134
 481.977        484.51          486.811         488.937         490.933
 492.83         494.656         496.429         498.166         499.882
 501.586        503.288         504.996         506.717         508.455

M= 1
UNDER           182.695         265.319         314.303         346.774
 369.934        387.336         400.939         411.91          420.987
 428.661        435.271         441.058         446.198         450.824
 455.037        458.915         462.52          465.902         469.101
 472.15         475.077         477.904         480.651         483.334

M= 2
UNDER           UNDER           103.539         185.49          239.745
 278.366        307.308         329.85          347.948         362.839
 375.345        386.032         395.305         403.459         410.715
 417.243        423.174         428.611         433.637         438.32
 442.715        446.866         450.812         454.585         458.213

M= 3
UNDER           UNDER           UNDER           UNDER           132.716
 186.798        227.28          258.762         283.987         304.692
 322.029        336.793         349.552         360.72          370.606
 379.449        387.433         394.702         401.372         407.539
 413.279        418.655         423.72          428.52          433.091

M= 4
UNDER           UNDER           UNDER           UNDER           UNDER
UNDER           147.252         187.674         220.026         246.545
 268.713        287.555         303.799         317.98          330.497
 341.655        351.692         360.793         369.108         376.758
 383.843        390.443         396.628         402.454         407.97

M= 5
UNDER           UNDER           UNDER           UNDER           UNDER
UNDER           UNDER           116.585         156.065         188.397
 215.397        238.316         258.046         275.241         290.388
 303.862        315.951         326.883         336.843         345.977
 354.407        362.232         369.536         376.388         382.849
STOP AT LINE 240

READY
```

APPENDIX C

LABORATORY REFERENCE NUMBERS FOR CHARTS

USED IN THE FIGURES

Figure Number	Laboratory Reference Number
3.1.1	26.4.71/3
3.2.4	20.12.73/1 and 20.12.73/5
4.1.1	29.4.71/1
4.1.2	Composite of 14.4.72/4, 14.4.72/5 and 14.4.72/6
4.2.1	Composite of 17.9.70/1, 17.9.70/3 and 17.9.70/4
4.3.2	20.3.73/3
4.3.3	20.3.73/5
4.3.4	20.8.73/1

VITA

Surname: NOBLE Given Names: MICHAEL RICHARD

Place of Birth: NEWPORT,WALES Date of Birth: MAY 29, 1945

Educational Institutions Attended,with Dates of Entering and Leaving:

LIVERPOOL COLLEGE OF TECHNOLOGY 1963 to 1968

Degrees, Diplomas, Etc., Awarded, with Dates and Names of Institutions:

H.N.C (Applied Physics)	1966	Liverpool College of Technology
Licentiate of the Institute of Physics	1967	Liverpool College of Technology
Graduate of the Institute of Physics	1968	Liverpool College of Technology

Honours and Awards:

Unilever Scholarship, 1967/68

Publications:

Barss,W. M. and Noble, M. R. 1973. Moiré Patterns in Underwater Acoustics. Paper presented at the 86th meeting of the Acoustical Society of America, Los Angeles, October 30-November 2.

PARTIAL COPYRIGHT LICENSE

I hereby grant the right to lend my thesis or dissertation (the title of which is shown below) to users of the University of Victoria Library, and to make single copies only for such users or in response to a request from the library of any other university, or similar institution, on its behalf or for one of its users. I further agree that permission for extensive copying of this thesis for scholarly purposes may be granted by me or a member of the University designated by me. It is understood that copying or publication of this thesis for financial gain shall not be allowed without my written permission.

Title of Thesis

Moiré Fringes in Underwater Acoustics

Author [redacted]

Signature

Michael Richard Noble

Name

April 29, 1974.

Date